Mechanical Design tools for patient specific management of Cerebral Aneurysms using CFD

Submitted by

Rishabh Saxena

for the award of the degree

of

Master of Technology

DEPARTMENT OF APPLIED MECHANICS

INDIAN INSTITUTE OF TECHNOLOGY MADRAS

CHENNAI-600036

JUNE-2022

DECLARATION

I declare that this written submission represents our ideas in our own words and where others' ideas or words have been included, I have adequately cited and referenced the sources. I also declare that I have adhered to all principles of academic honesty and integrity and have not misrepresented or fabricated or falsified any idea/data/fact/source in our submission.

Place: Chennai

Date: 03-June-2022

Signature

Rishabh Saxena

BT20M026

THESIS CERTIFICATE

This is to certify that the thesis entitled **"Mechanical Design tools for patient specific management of Cerebral Aneurysms using CFD."** submitted by **Rishabh Saxena** to the Indian Institute of Technology, Madras for the award of the degree of **Master of Technology** is a bona fide record of research work carried out by him under my supervision. The contents of this thesis, in full or in parts, have not been submitted to any other Institute or University for the award of any degree or diploma.

Guide (s):

Dr. Prasad Patnaik BSV
Professor, Department of Applied Mechanics
Indian Institute of Technology Madras
Chennai – 600036

Dr. Jayanand Sudhir B
Associate Professor, Department of Neurosurgery
Sree Chitra Tirunal Institute of Medical Sciences and Technology
Trivandrum – 695 011

Place: Chennai

Date: 03/06/2022

ACKNOWLEDGEMENTS

I am deeply indebted to Dr. Prasad Patnaik B.S.V. and Dr. Jayanand Sudhir B for their inspiration, constant support, and guidance throughout this project. AM6535 Course taught by Dr. Prasad Patnaik B.S.V. and Dr. Arun K. Thittai helped me to build concepts related to Imaging Aided Bio-Fluid and CFD. I am thankful to Dr. Jayanand Sudhir B for providing the opportunity to observe real-time surgical intervention of the aneurysm and for sharing important clinical insights. I would like to express my gratitude to Dr. Bhushan Akhade, Mr. Satyajit Choudhary, and Mr. Nikhil Yewale for their help and support in providing DICOM data, 3D unstructured grid generation, hemodynamic results, and discussion respectively. I would like to extend my thanks to Mr. Valeti Chanikya and Mr. Pankaj Baraiya for many insightful discussions. I thank my faculty advisor, Dr. Manoj N, for his constant guidance and support also grateful to MHRD for supporting my MTech in Clinical Engineering (Dept. of Biotechnology) and MTech. project under the Department of Applied Mechanics at IIT Madras, Chennai.

ABSTRACT

Keywords: Anterior Communicating Artery Aneurysms (ACOM), CFD, 3D unstructured mesh, rupture risk, symmetric inlet, A1 asymmetric ACOM

Aneurysms are pathological expansions of an arterial wall, which are formed at different locations such as, bifurcations and side walls. In the cerebral circulation, aneurysms typically occur at a number of locations such as, middle cerebral artery, basilar, anterior/posterior communicating artery etc. The rupture risk of Anterior Communicating Artery Aneurysms (ACOM) has been known to be higher than that of aneurysms at other locations. Thus, this study aims to investigate the hemodynamic parameters associated with risk factors for the rupture of ACOM aneurysms. The aneurysm and blood vessels were segmented from Computed Tomography (CT) angiography to prepare a Computational fluid dynamics-based model for simulations. Patient-specific computational fluid dynamics (CFD) calculations are performed to simulate and analyze the aneurysm flow. Generation of good quality 3D unstructured meshes is necessary to accurately resolve complex fluid dynamical activity and systematically enable grid independent studies which resolve the physiologically relevant flow features. In this study, we compared the important hemodynamic parameters of symmetric inlet and A1 asymmetric (dominant) ACOM aneurysms and assessed the rupture risk.

TABLE OF CONTENTS

LIST OF FIGURES

LIST OF TABLES

ABBREVIATION

NOTATIONS

D : Diameter of normal artery.....25

P : Absolute Pressure [Pa].....10

U : Velocity in z-direction 25

u, v, w : Velocity component in the axial, radial and tangential directions, respectively 10

U_t : Time varying inlet velocity [m/s].....25

ϑ : Kinematic viscosity [3.3×10-6 m2/s for blood] 10

ρ : Fluid density [1060 kg/m3 for blood].....10

CHAPTER 1

INTRODUCTION

1.1. INTRODUCTION

A cerebral aneurysm is a vascular malformation in the brain's arterial circulation which involves the weaking of vessel wall that is more prone to rupture [1]. This rupture may cause a subarachnoid haemorrhage bleeding into the space between the skull bone and the brain. Typical Computed Tomography (CT) based angiogram, indicative of cerebral circulation is shown in **Fig. 1.1**. The most common location for brain aneurysms is in the network of arteries at the base of the brain called the Circle of Willis (see **Fig. 1.2**).

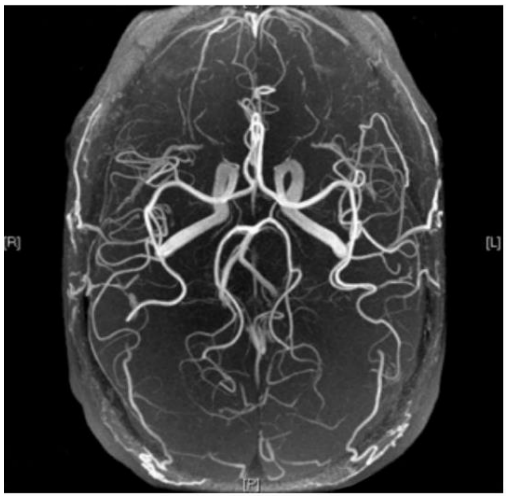

Fig. 1.1: Brain CT Angio

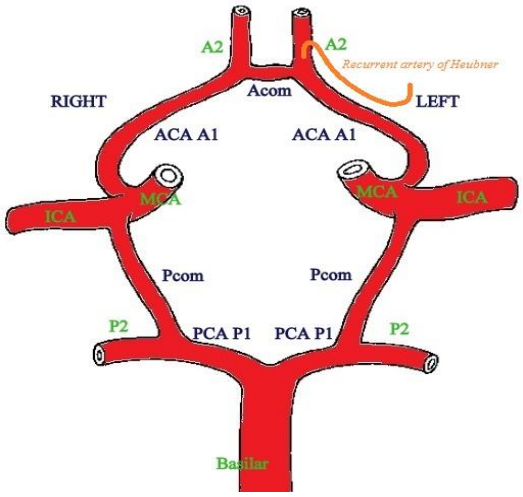

Fig. 1.2: Circle of Willis with Aneurysm Sites

Fig. 1.3: ACOM Aneurysm during Surgery

In most of the cases, cerebral aneurysms go unnoticed until they rupture or are detected by brain imaging that may have been obtained for another condition. The anterior communicating artery is one the most common locations for aneurysm development. The ACOM artery is a common site of Intracranial Aneurysms (IAs), accounting for 35% of all ruptured aneurysms [2]. The ACOM artery is the only cerebral artery that evolves from an arterial plexus in the interhemispheric fissure, which results in a high frequency of vascular anomalies such as fenestration and duplication. Because of the complexity and diversity in the geometry of the ACOM, these are considered the most complex among the anterior circulation (see **Fig. 1.3**). ACOM aneurysms are responsible for about 39% of aneurysmal subarachnoid hemorrhage cases. It receives blood from both carotid circulations. Detection methods are used to pinpoint the location, size, type, and any other characteristics of the aneurysm that will help the doctors make the best decisions about how to move forward. Based on the characteristics of CT Angio, 3D Slicer software is used to segment the brain CT images. 3D Slicer is a free open-source software package used for 3D patient-specific model extraction. Its application scope is mainly the analysis and research of medical images, aiming at realizing the visualization of medical images.

Patient-specific computational fluid dynamics (CFD) aided by the aforementioned imaging techniques, is emerging as a standard tool to simulate and analyze the aneurysm blood flow. Morphological parameters extracted from the medical imaginary methods can give a reliable estimate of hemodynamic conditions for the patients. It can assist physicians to quantify to a greater extent, some phenomena that are difficult to capture with in vivo imaging techniques, through the use of CFD to simulate the flow via patient-specific geometries. Image-aided CFD calculations can offer specific data on the flow fields and hemodynamic parameters affecting blood vessels with temporal and spatial resolutions exceeding the ones of the in vivo techniques. A better understanding of hemodynamic can improve diagnosis and treatment [3] The meshing process of the geometry is conducted purposely to build a discretized system of fluid flow equations and estimate the flow fields for the whole model. High Mesh density was maintained in the vicinity of the aneurysm wall to capture greater details, while the mesh face is intended to display the mesh edge effect. Generation of good quality tetrahedral meshes for cerebral aneurysm blood flow simulation starting from low-quality triangulations obtained from the segmentation of patient-specific medical images is both an art and technically daunting. Two important elements have to be taken into account to generate a high-quality tetrahedral mesh for cerebral aneurysm blood flow simulations from medical images:

(i) Quality of triangular surface mesh and

(ii) Capability to generate boundary layers meshes.

Based on the literature review presented in Chapter 2, it was noticed that detailed and systematic simulations that directly correlate the mesh quality against complex patient specific geometries are missing in the literature. To this end, the following objectives is formulated

- To perform Computational Fluid Dynamics (CFD) simulations to systematically study the hemodynamic parameters of clinical interest vis-à-vis mesh quality.

Specific emphasis was accorded to anterior communicating artery aneurysms.

1.2. ORGANIZATION OF THE THESIS

- In the 2nd chapter, Literature review covering the summary of unstructured mesh generation and CFD techniques on patient-specific aneurysm model is presented. Further Hemodynamic parameters, and rupture risk prediction theories on ACOM aneurysm are discussed.
- In 3rd chapter, the solution Methodology, Mesh Generation and CFD simulations are broadly discussed. Numerical details about meshing Algorithms (Octree and Delaunay), Prism Mesh creation, Meshing Strategy, Grid Independence results, CFD details are presented.
- In the 4th chapter, definitions and numerical equations for important hemodynamic parameters are included and a comparison of symmetric inlet ACOM (unruptured) and A1 asymmetric ACOM complex are explained with illustrations.
- 5th chapter presents conclusions and future scope.

CHAPTER 2

LITERATURE REVIEW

2.1. INTRODUCTION

Possible cause of cerebral aneurysm formation and the role of CFD

The process of aneurysm formation is not fully elucidated, Tanaka et al. proposed that chronic inflammation of the cerebral arteries is due to genetics and molecular biology which is closely associated with the pathogenesis of cerebral aneurysm initiation. Blood flow characteristics were found to affect chronic inflammation of the cerebral arteries, besides smoking, ingesting alcohol, and decreased estrogen levels [4]. W. Kaspera et al. found that degenerative lesions caused by hemodynamic stress play an important role in cerebral aneurysms initiation. Animal studies showed that exposure to hemodynamic stress associated with an increased blood flow leads to degenerative changes of the internal elastic lamina and muscularis media of the arterial wall immediately adjacent to the apex of bifurcation and aneurysm formation [5]. According to Murayama et al., Image-aided computational fluid dynamics provide a better understanding to identify the mechanism responsible for the formation, growth, and rupture of aneurysms. These techniques facilitate the possible ways to improve the diagnosis and evaluation of patients by including hemodynamic information with already available anatomical data. Also, CFD techniques play a significant role in endovascular treatment planning and endovascular device designing [1].

Importance of good quality mesh generation in Imaging Aided CFD:

Marchandise et al. proposed that to imply CFD simulation techniques in patient-specific geometries robust mesh generation is necessary. The accuracy and efficiency of numerical methods depend upon the quality of mesh created. Researchers have studied the impact of mesh quality in patient-specific geometries. Mesh quality parameters such as aspect ratio, orthogonality, skewness, smoothness, etc indicate whether the mesh is suitable for computation or not. The presence of badly shaped cells makes an unsuitable mesh and increases the local effective spatial discretization error [6]. The advancing layer method is used to create the triangulated surface mesh. And, then Unstructured Isotropic tetrahedral meshes are used with sufficiently small elements near the wall to resolve the boundary layer and capture accurately derived quantities such as WSS, OSI, RRT, etc. The most common cause for failure of

computational meshes in 3D problems is insufficient spatial resolution, leading to inaccurate computation of local velocity and wall shear stress features. For this reason, demonstration of mesh-independence is advocated in computational fluid dynamics (CFD). Prakash and Ethier et. al has performed mesh independence on the Right Coronary Artery (RCA) model by creating conventional high-resolution unstructured mesh and adaptive mesh series. It is found that using adaptive mesh series, a large number of nodes were needed to achieve mesh independence in the Wall Shear Stress (WSS) field. This translates into a significantly greater error when computing Wall Shear Stress Gradient (WSSG) [7] .

Study on the implementation of Image Aided Computation Fluid Dynamics (CFD):

High-resolution image is acquired from imaging techniques such as digital subtraction angiography (DSA) or CT angiography are used to conduct CFD analysis. In CFD analysis of cerebral aneurysms, Murayama et al. considered blood as a Newtonian fluid with specific values of density and viscosity. In flow analysis, the flow field was mostly assumed to be incompressible laminar flow because the Reynolds number (based on vessel diameter and flow speed) was in the range of several hundred. After applying computational preconditions, including assumed blood material properties and boundary conditions, the blood flow was simulated, solving the 'Navier–Stokes' equations[1]. Nanduri, Pino-Romainville, and Celik et al., followed the procedure for patient-specific modelling and characterization of cerebral aneurysms from angiogram images and concluded that flow patterns are independent of the mean flow velocity and viscosity but are highly dependent on the geometry. This finding makes the accurate reconstruction of the geometry more critical [8].

A study comprising the relation between ACOM formation and A1 Asymmetry:

Anterior Communicating Artery (ACOA) is one of the most frequent sites of aneurysm formation, which accounts for nearly one-fourth of all aneurysms. Due to its diverse and complex geometry researchers have studied its local hemodynamic environment for aneurysm initiation, growth, and possible causes of rupture. Kwak et al. has found that Aneurysms of the ACOM complex are more likely to have A1 asymmetric complex segments. Single A1 vessel dominance in patients with ACOM aneurysms was observed to be as high as 68% [9]. Jabbarli et al. studied a total of 594 patients are included in the study, out of which 227 patients have ruptured ACOM and a total of 107 ACOM aneurysms have A1 Asymmetry. This correlation indicates a causative role for A1 asymmetry in the formation of ACOM aneurysms. Few studies indicate that asymmetrical local inflow causes chronic hemodynamic stress on the walls of the

ACOM [10]. Castro et al. studied the role of flow patterns in rupture history. There are 4 types of flow inside ACOM aneurysms. Type 1, type 2, type 3, and type 4 inflow refers to the stable inflow jet direction with a single vortex, the stable direction of the inflow jet with 2 or more unchanging vortices, changing the direction of the inflow jet with the creation or destruction of a single vortex during the cardiac cycle, and changing the direction of the inflow jet with multiple varying vortices respectively. Twenty-six ACOM aneurysm models were included in the study out of which 11 had asymmetric A1 complex and other 15 had symmetric inlets. It is concluded that Aneurysms with small impaction zones have higher flow rates entering the aneurysm this elevates MWSS and finally caused the rupture [11]. Few studies indicate that low or stagnant flow can result in an inflammatory response in the vascular wall and low WSS is associated with IAs rupture in posterior circulation aneurysms and ACOM aneurysms [12]

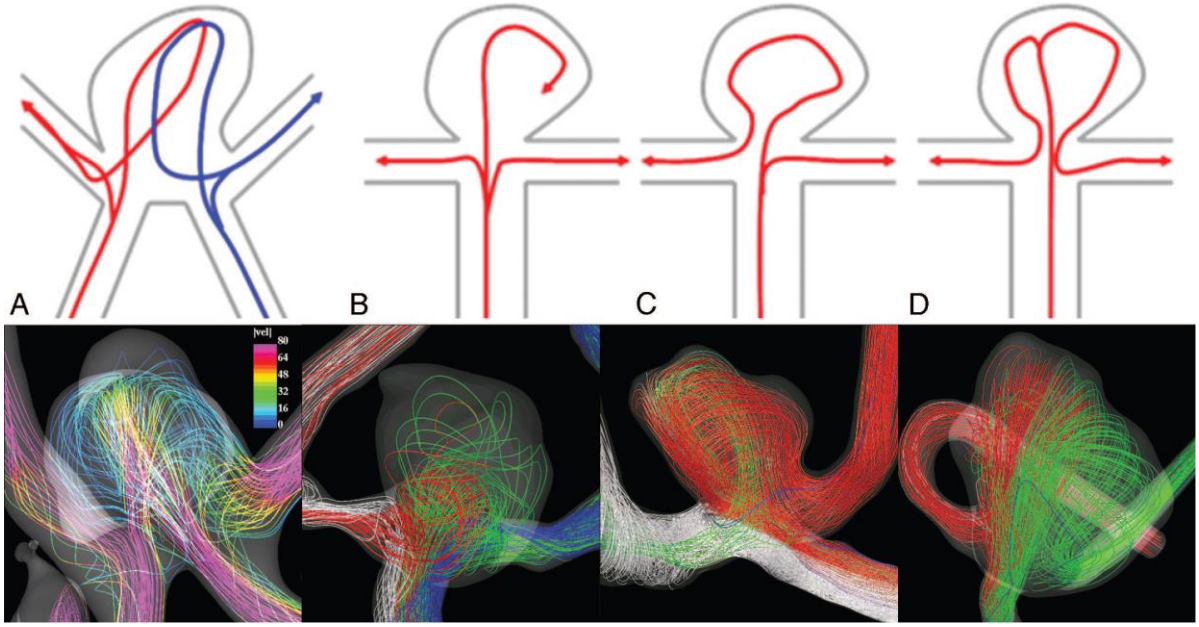

Fig. 2: A–D, Different flow patterns found in ACOM aneurysms are shown in the top row. Pictures of the streamlines colored by the magnitude of the velocity and their path from the A1 segment to the A2 segments in 4 selected aneurysms for each flow type [11].

Study of Hemodynamic parameters for rupture risk assessment of cerebral aneurysms

Researchers performed CFD analyses and statistical tests for a total of 173 and 204 aneurysms, respectively, including ruptured and unruptured aneurysms. It is reported in the study that aneurysmal rupture had a strong relation to hemodynamic and morphological parameters, such

as low WSS, high OSI, and size ratio. Some studies reported that the blood flow impingement on the aneurysmal wall produced high WSS which is the main reason for aneurysms rupture. Meng et al. proposed the implications of high and low WSS on the aneurysm. High WSS at the blood flow jet impingement zone is responsible for the initiation of aneurysms. After aneurysm initiation, its growth process differs depending on whether WSS is high or low. Due to high WSS, degeneration of the cellular matrix and cell apoptosis takes place, and finally, aneurysms will rupture even if they are small in size. However, if the WSS is low, the aneurysm may become larger because the inflammation caused by slow recirculation and a disturbed flow environment promotes the formation of atherosclerotic plaques, which exacerbate the effects on inflammatory cells. Finally, aneurysms will rupture or stabilize depending on the temporal and spatial WSS alterations accompanied by geometrical changes of the aneurysms [13]. In most of the studies, images taken after their rupture and CFD has been performed on reconstructed geometries. Such studies were based on the assumption that ruptured and unruptured aneurysms have a different value in CFD parameters. CFD analysis on images that were taken before and after rupture showed that the aneurysm shape hychanges due to rupture caused a 20%–30% chance of WSS [1].

2.2. THESIS FOCUS

Researchers have explored various morphological and hemodynamic parameters associated with rupture risk of cerebral aneurysm. But many of the studies focus on rupture risk prediction in Intracranial Aneurysm (ICA), Middle Cerebral Aneurysm (MCA), and Anterior Communicating Aneurysm (ACOM) based upon mainly morphological indicators or few hemodynamic parameters (WSS, OSI, etc.). Rupture risk in Internal Carotid Artery Aneurysm (ICA) have been investigated by many researchers as it offers a simple bifurcation geometry. The Anterior Communicating artery complex is also one of the most common locations for aneurysm development. The ACOM complex has a H-shaped configuration with 2 inlets and 2 outlets posing a unique challenge for CFD studies. According to a study 18-24% of aneurysms are detected in this site which is a large fraction of total aneurysms detected. So, the focus of the current study is exclusively on ACOM aneurysms. The aim of the study is to generate good quality 3D unstructured tetrahedral mesh and compare the hemodynamics of ACOM aneurysms having symmetric vs A1 asymmetric ACOM complex.

CHAPTER 3

GOVERNING EQUATIONS AND METHOD OF SOLUTIONS

3.1. Governing Equations

The mathematical model that governs the fluid flow through the anterior communicating artery (ACOM) of interest are presented. Detailed solution methodology through the numerical calculations is briefly presented.

The conservation of mass and conservation of momentum equations (popularly known as Navier-Stokes) describe the blood flow through the arteries of concern. The partial differential equations for the incompressible, unsteady and Newtonian approximation are given as,

$$\frac{\partial u}{\partial x}+\frac{\partial v}{\partial y}+\frac{\partial w}{\partial z}=0 \tag{3.1}$$

$$\frac{\partial u}{\partial t}+u\frac{\partial u}{\partial x}+v\frac{\partial u}{\partial y}+w\frac{\partial u}{\partial w}=-\frac{1}{\rho}\frac{\partial P}{\partial x}+\vartheta\left(\frac{\partial^2 u}{\partial x^2}+\frac{\partial^2 u}{\partial y^2}+\frac{\partial^2 u}{\partial z^2}\right) \tag{3.2}$$

$$\frac{\partial u}{\partial t}+u\frac{\partial u}{\partial x}+v\frac{\partial u}{\partial y}+w\frac{\partial u}{\partial w}=-\frac{1}{\rho}\frac{\partial P}{\partial x}+\vartheta\left(\frac{\partial^2 u}{\partial x^2}+\frac{\partial^2 u}{\partial y^2}+\frac{\partial^2 u}{\partial z^2}\right) \tag{3.3}$$

$$\frac{\partial u}{\partial t}+u\frac{\partial u}{\partial x}+v\frac{\partial u}{\partial y}+w\frac{\partial u}{\partial w}=-\frac{1}{\rho}\frac{\partial P}{\partial x}+\vartheta\left(\frac{\partial^2 u}{\partial x^2}+\frac{\partial^2 u}{\partial y^2}+\frac{\partial^2 u}{\partial z^2}\right) \tag{3.4}$$

Where u, v, and w are the velocity components in the x, y, and z direction P is pressure, ρ is Density and ϑ is kinematic viscosity. These equations are discretized and solved at each nodal point for a mesh created on the domain of interest. Furthermore, for the application of CFD in cerebral aneurysms, If a steady-state condition is applied these equations simplify even more resulting in a much smaller computational time.

3.2. Numerical Methodology

For better understanding hemodynamics of blood flow, it is very essential to analyze a realistic geometric model. Using current technologies, it is possible to convert clinical raw image data into a realistic geometric model. Angiograms obtained from medical imaging techniques like Magnetic Resonance Imaging, and Computerized Tomography scans are smoothened, and segmented and the surface is generated by using 3D tools like 3D slicer. The output is in form of .STL file which is imported in Mesh generation software. ICEM-CFD is used for mesh generation.

It is difficult to achieve a structured mesh for complex geometries like aneurysms and manage blocks around them. The preferable option is to generate an unstructured mesh with Tetra and Prism elements. Using the Octree method Tetra mesh is generated and Prism layers are provided at the interface to capture the boundary phenomenon. More Prism layers are provided at the interface and coarse tetra mesh away from the interface to save computational time. The solid part of the Aneurysm wall is extruded based on the uniform thickness required. Conformal mesh is used to transfer data easily between flow and structure. Walls are assumed rigid and have no slip. Based on the temporal stability, an adaptive time-step is adopted for the unsteady incompressible flow solver. For CFD simulations, the computer cluster provided by IIT Kanpur included 8 nodes for which there were 20 processers each. The Open Foam v-1912 community solver was chosen for the simulations. Open Foam is a solver that couples finite element and finite volume methods to solve the Navier-Stokes equations. ADINA and ANSYS Fluent are also popular commercial solver in CFD. Ansys ICEM-CFD is used for unstructured meshing in the present study. Other than this VMTK and Gambit are optional meshing software.

3.3 Mesh Details

In CFD techniques, the simulation of the patient-specific flow domain has necessitated the demand for robust grid generation techniques to characterize complex geometries. The domain is discretized into a finite set of control volumes or cells. The discretized domain is called the "Grid" or the "Mesh." Grid elements are created to fill the volume for simulation. Each element of the mesh represents a discrete space that governs the flow locally. Mathematical equations that represent the flow physics are then applied to each cell of the mesh. The final result is the ability to store time-dependent flow properties such as pressure, and velocity in each cell.

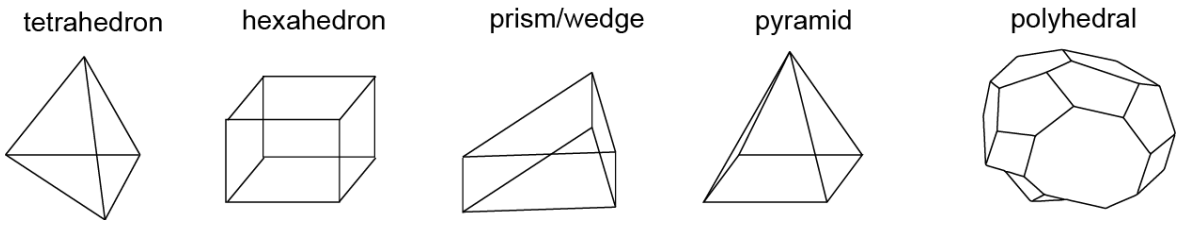

Fig. 3.1: Types of mesh elements

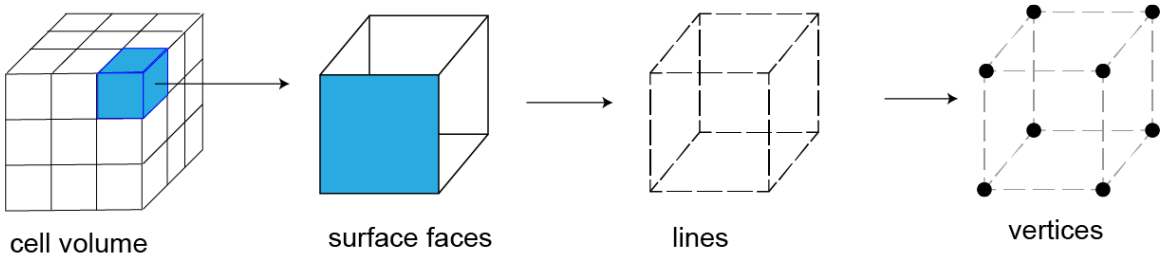

Fig. 3.2: Mesh Hierarchy

Generating a high-quality mesh is extremely important to obtain reliable solutions and to guarantee numerical stability. The quality of the meshes is of great importance since it impacts both the accuracy and the efficiency of the numerical method.

Mesh Type: Mesh elements/cells are generally hexahedral, tetrahedral, square pyramids (pyramids, extruded triangles, wedges, or triangular prisms), or polyhedral (see **Fig. 3.1**). It is useful to envision the mesh topology as a hierarchical system, where higher topology assumes the existence of topologies beneath it. 3D cell inherits the lower topologies, i.e., a volume is made up of faces, a face is made from lines, and a line is made from vertices (see **Fig. 3.2**). A common meshing approach is to use a bottom-up approach, where firstly vertices, lines, and faces (from the segmentation step) are created to form a surface mesh and subsequently fill the enclosed volume with 3D cells, i.e., the mesh elements.

Structured Vs Unstructured Meshes: Structured mesh has the advantage that its layout is simple due to the direct connections between adjacent cells. For example, a three-dimensional cell is connected by six neighbouring cells with points easily accessible by triple indices (i, j,

k) incrementing or decrementing with each adjacent cell. This indexing makes CFD solvers simple to program and leads to a small memory footprint. However, the creation of structured meshes for complex geometries such as patient-specific geometries is highly time-consuming as it involves a lot of manual work. Therefore, in most literature, unstructured tetrahedral, hexahedral, or polyhedral meshes are used. An unstructured mesh has the advantage that it is much more suited to fit within complex shapes. Furthermore, the volume filling can, e.g., be performed automatically using a Delaunay triangulation or a hierarchical approach.

In the near-wall region, both types of meshing algorithms need to achieve a resolution that has reasonable accuracy in resolving boundary layer flows. This is achieved by either adding prism layers along walls or by hierarchically refining Tetrahedral cells.

Unstructured Meshes: The Cerebral circulation geometry is highly irregular and does not fit exactly to orthogonal lines or Cartesian coordinates. The surface can internally be filled with the 3D unstructured elements of the same kind or can be a hybrid mix of different elements including structured and prism layers. An unstructured grid is typically identified by irregular connectivity. To store the data for the computation, new data structures, e.g., edge-based, face-based, or cell-based structures are needed to hold the connectivity scheme. A node of a cell can be connected to any number of nodes from its neighbours, which may lead to complex connectivity dependencies. The descriptions of some of these connectivity algorithms include Delaunay, advancing front, quadtree/octree, etc.

Unstructured CFD meshing technologies have matured and their use has become more prevalent with commercial CFD vendors. They provide the user with simpler automated methods for achieving a meshed model and a user-friendly interface.

Two important elements have to be taken into account to generate a high-quality tetrahedral mesh for patient specific ACOM aneurysm from the 3D segmented model:

I. The quality of the triangular surface mesh.
II. The capability to generate boundary layer meshes.

Unstructured Mesh Creation in Patient Specific Aneurysm Model Using ICEM CFD tools:

- The 'Import Model' option allows us to use the Workbench Readers to import geometry or mesh data into ANSYS ICEM CFD.
- In the Geometry, the option use the repair geometry tool and build a diagnostic topology
    - Build Topology builds curves and points, which will help to diagnose the model for geometrical problems. The curves will automatically take on colors to show their association with adjacent surfaces.
    - Repair any gaps or holes in the topology.

Extruded the inlets and outlets:

- Create three points using the screen select option in the geometry section.
- Create a circle by using the center point and 2 points in the arc (this option will reflect in Create and modify curve).
- We are extruding 3D distance by creating explicit location points and joining the curve with the loft surface option and closing the inlets and outlets using a simple surface.

Now by splitting the aneurysm dome with its inlet and outlets so that it can create higher resolution mesh over the aneurysm dome and can capture more hemodynamic details. After this we will create a body using Create Body option in our case fluid will flow inside the arteries. After naming the parts. We will choose Mesh Option:

Global Mesh Setup provides the general and specific meshing algorithm parameters used for the various meshes. We will define scale factor, Max element, Min element, and refinement levels. After Grid Independence these parameters will be fixed for the geometry (**Table 3.1**), These parameters define as follows:

- **Scale Factor:** It multiplies other mesh parameters to globally scale the model. The Global Element Scale Factor can be any positive real number, and it allows, globally control of the mesh size instead of changing the mesh parameters for different entities.
- **Max Element**: It controls the size of the largest element. The largest element size in the model will not exceed the multiplication of the Max Element size and Global Element Scale Factor.

- **Curvature/Proximity Based Refinement:** Using this option the mesh is automatically refined based on geometry curvature and proximity. This will result in larger elements on flat planar surfaces and smaller elements in areas of high curvature or within small gaps. The algorithm attempts to satisfy the refinement and elements in gap settings but is limited by the minimum size limit**.**
- **Min size limit:** specifies the size limit for the smallest element. Mesh elements will be prevented from being subdivided smaller than this value. If, however, the refinement and elements in gap settings are satisfied without refining down to this minimum size, refinement will stop on its own and may never subdivide down to this Min size limit value.
- **Refinement** defines the number of edges that would fit along a radius of curvature if that radius were extended out to 360 degrees. This is generally used to avoid having too many elements along a given curve or surface if the Min size limit is too small for that particular curve.

Scale Factor	Max Element(M)	Min Element	Refinement
0.66	R/4	M/5	20

Table 3.1: Global Mesh Parameters

Volume Meshing Parameters: It defines Volume Mesh Type i.e., Tetra/ Mixed, Hexahedral, Cartesian, and Meshing Method like Octree, Delaunay, Advancing Front.

- The **Robust (Octree)** option will generate a tetra mesh using a top-down meshing approach. An Octree mesh does not require surface mesh, it will generate automatically in ICEM-CFD software. Also, It accepts a variety of parameters in a more general way. This algorithm ensures refinement of the mesh where necessary, but maintains larger elements where possible, enabling faster computation. Once the "root" tetrahedron, which encloses the entire geometry, has been initialized, Tetra subdivides the root tetrahedron until all element size requirements are met.
- The **Quick (Delaunay)** option will generate a tetra mesh using a bottom-up meshing approach (Delaunay Tetra algorithm). This algorithm requires an existing, closed surface mesh. If this has not yet been created, it will automatically create the surface mesh from the geometry as defined by the Global Mesh Setup settings (or the Surface

Mesh option). The volume mesh will then be generated from this surface mesh. You can also run this in two steps by creating/importing a surface mesh first and then running these meshes.

- The **Smooth (Advancing Front)** option will generate a tetra mesh using a bottom-up meshing approach using the Advancing Front Tetra meshes. The surface mesh will be created as defined by the Global Mesh Setup settings (or Surface Mesh option). The volume mesh will then be generated from this surface mesh. This meshing method results in a more gradual change in element size. The initial surface mesh should be of fairly high quality.

Prism Meshing Parameters: Prism layers are used to capture boundary layer flow features. No. layers can be increased or decreased by varying Initial height, Height ratio. These Prism Parameters should be evaluated based upon the grid- the independence test (see **Table 3.2**).

- **Growth Law:** determines the height of the layers given the initial height and height ratio. There are different laws available in ICEM CFD e.g., Linear, Geometric, and Exponential (see **Fig. 3.3**). In the present study geometric growth law is used for generating prism layers.

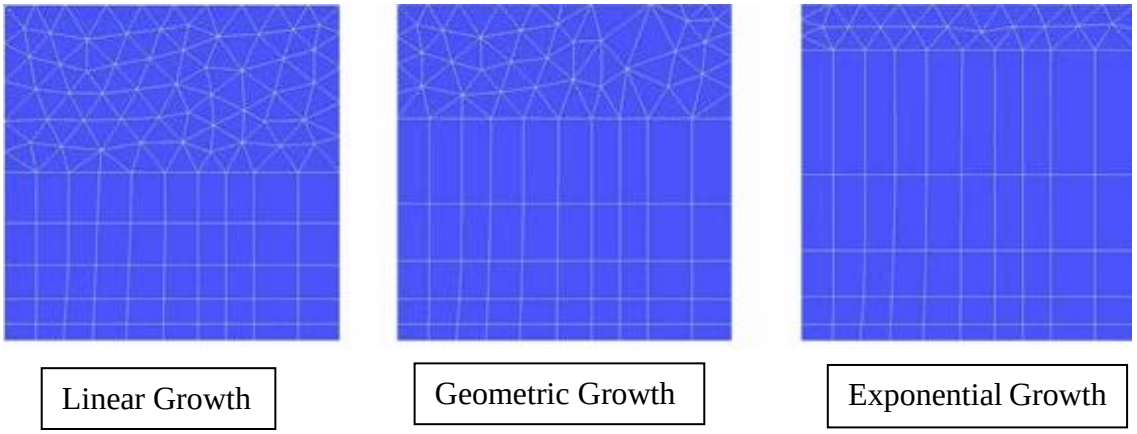

Fig. 3.3: Prism Growth Layers

- **Initial Height:** is the height of the first layer of elements.
- **The height ratio** is the expansion ratio from the first layer of elements on the surface. This ratio will be multiplied by the element height of the previous layer to define the height of the next layer.
- **The number of layers** is the number of layers to be grown from the surface or curve.

Initial Height	HR	Total Height	Aneurysm Max height
M/10	1.2	0.2R	M/2

Table 3.2: Prism Parameters

Part Mesh Setup: Using this function, we can control all mesh parameters:

- A value of 0 entered for a Part level setting causes the global parameter value to be used.
- Part level settings will override Global settings where appropriate. See the detailed description for each parameter.
- Entity level settings, for example on a surface or curve, will override Part level settings where appropriate.

Compute Mesh: The Compute Mesh option allows for to generation of the mesh specified by the meshes and various parameters.

- **Edit Mesh:** The Edit Mesh menu contains all of the operations necessary to manipulate, check, improve the quality of the mesh and fix any problems.
- **Check Mesh:** The Check Mesh option allows to locate problems with the mesh that will usually lead to failure when translating or running the solution. Errors will most likely fail to write out the mesh or read it into the solver. Possible Problems may lead to solution crashing or diversion. We can select any combination of errors and possible problems to check at one time.

Finding the Quality of Mesh: The Display Mesh Quality option runs a diagnostic check of individual element quality. Mesh Quality can be displayed by a histogram. The mesh quality criteria available are described in the following sections:

- The quality is calculated differently for different element types, For The tetrahedral elements quality is calculated as the aspect ratio of the tetra element and for prism, the quality is calculated as the minimum of the Determinant and Warpage. Warpage is normalized to a factor between 0 to 1, where 90 degrees is 0, and 0 degrees is 1.

- **Aspect Ratio:** ANSYS ICEM CFD calculates the ratio between the volume of the element and the radius of its circumscribed sphere power three. The values are scaled, so that an aspect ratio of 1 corresponds to a perfectly regular element, while an aspect ratio of 0 indicates that the element has zero volume.

$$Aspect\ Ratio = \frac{\left(\frac{Volume\ (V_{act})}{(Circumscibed\ Radius(R_{act})^3)}\right)_{Actual}}{\left(\frac{Volume\ (V_{Ideal})}{(Circumscibed\ Radius(R_{Ideal})^3)}\right)_{Ideal}}$$

- **Skewness:** It calculates the maximum skewness of an element. The skewness is defined differently for volume and surface elements. In all cases, it is normalized so that 1 is ideal and 0 is the worst possible. Skewness is defined as the normalized worst angle between each of the 6-face normal and the vector defined by the centroid of the hexahedron and the center of the face (see **Fig. 3.4**).

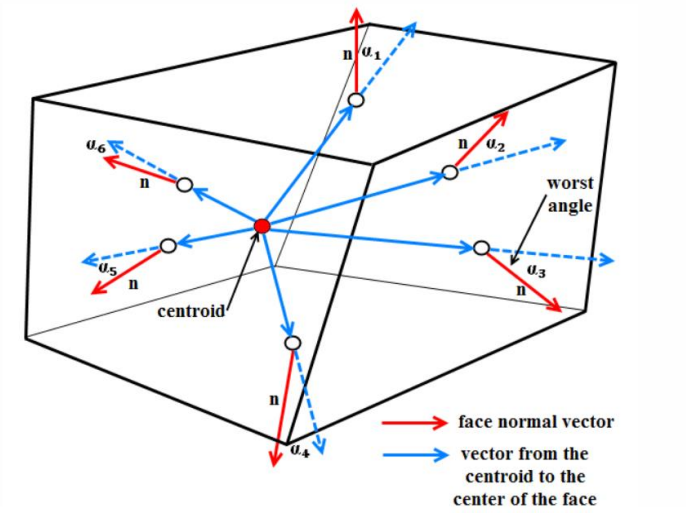

Fig. 3.4: Skewness

- **Non-Orthogonality**: It involves the angle between the vector that joins two mesh (or control volume) nodes (s) and the normal vector for each integration point surface (n) associated with that edge. Always it is better to spend more time in getting a good quality mesh, maybe with non-orthogonally as less as possible depending on software (For example less than 60 in Open FOAM) (see **Fig. 3.5**).

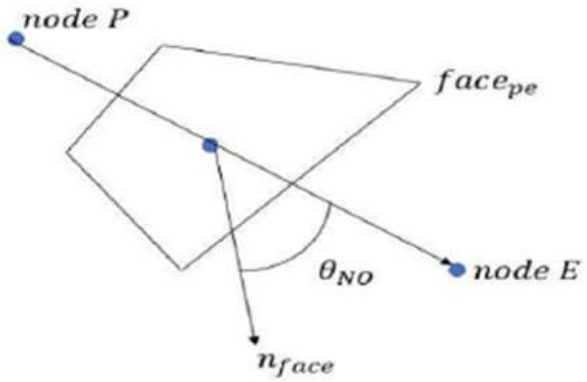

Fig. 3.5: Non-Orthogonality

- **Smoothening:** The Smooth Mesh Globally option allows you to automatically improve the quality of the mesh elements. Different smoothing algorithms are available depending on which mesh type is loaded. Mesh can be smoothed to a particular quality criterion and with a specified number of iterations to achieve a given quality level. A mesh containing tetras, pyramids, prisms, and triangular and quad surface elements can be smoothed. Smoothening Iterations specify the number of iterative steps. Each iteration will apply to smooth a percentage of the elements below the specified quality. The more iterations, the smaller the percentage of elements that are selected and incremented for each step. For example, if 5 iterations are specified, the first iteration will smooth the worse 20% of elements, the second will smooth 40%, etc. Increasing the number of iterations is more robust, but fewer iterations mean that each iterative step smoothens more elements each time.

After smoothening and getting desired quality (In our case min 0.45 is required for all mesh sizes), we will convert it into a **.MSH file** by using the output mesh option.

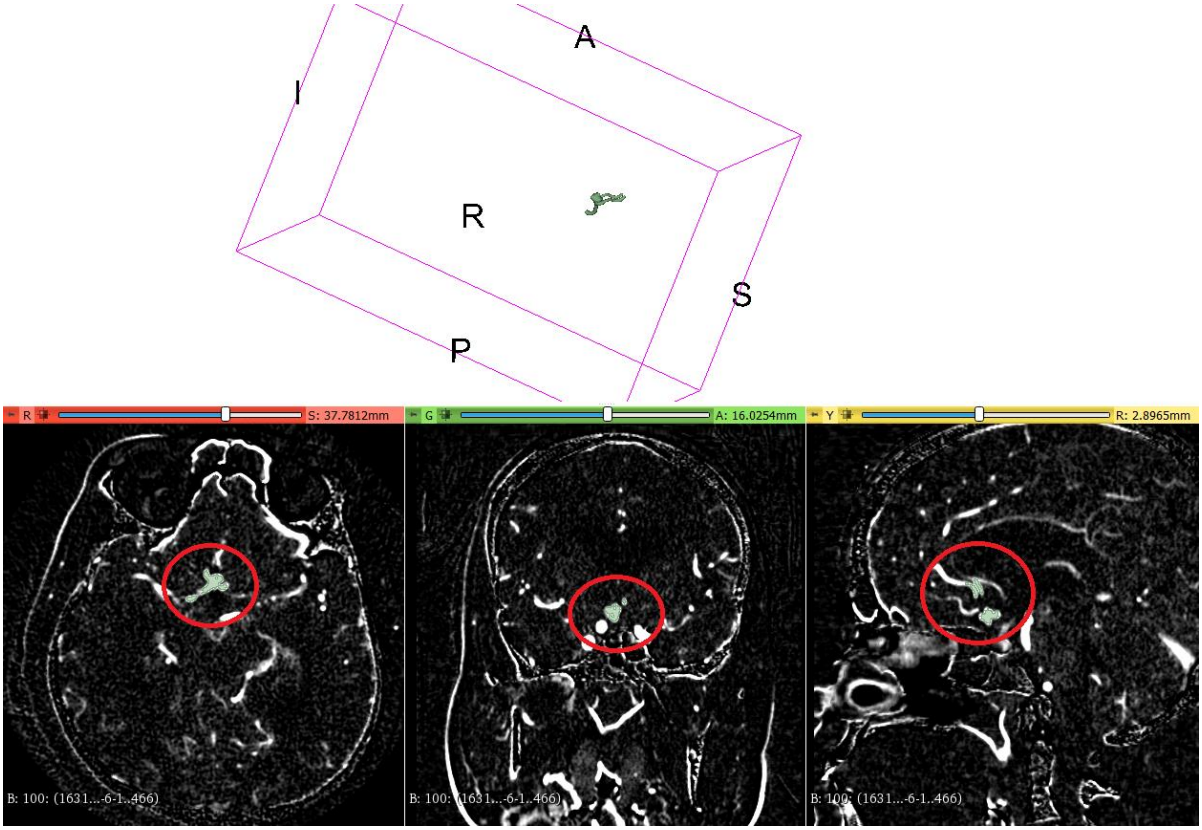

Fig. 3.6: Red Circle is indicating thresholding on DICOM data aneurysm site

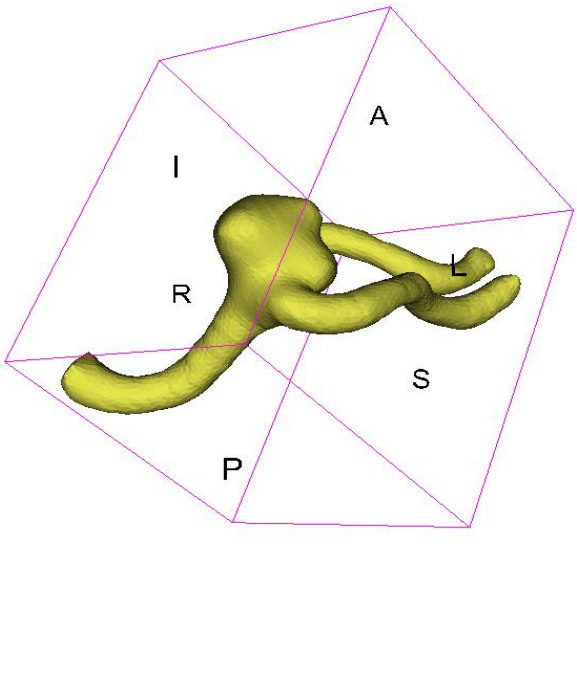

Fig. 3.7: 3D model Generation and Converting into .stl format

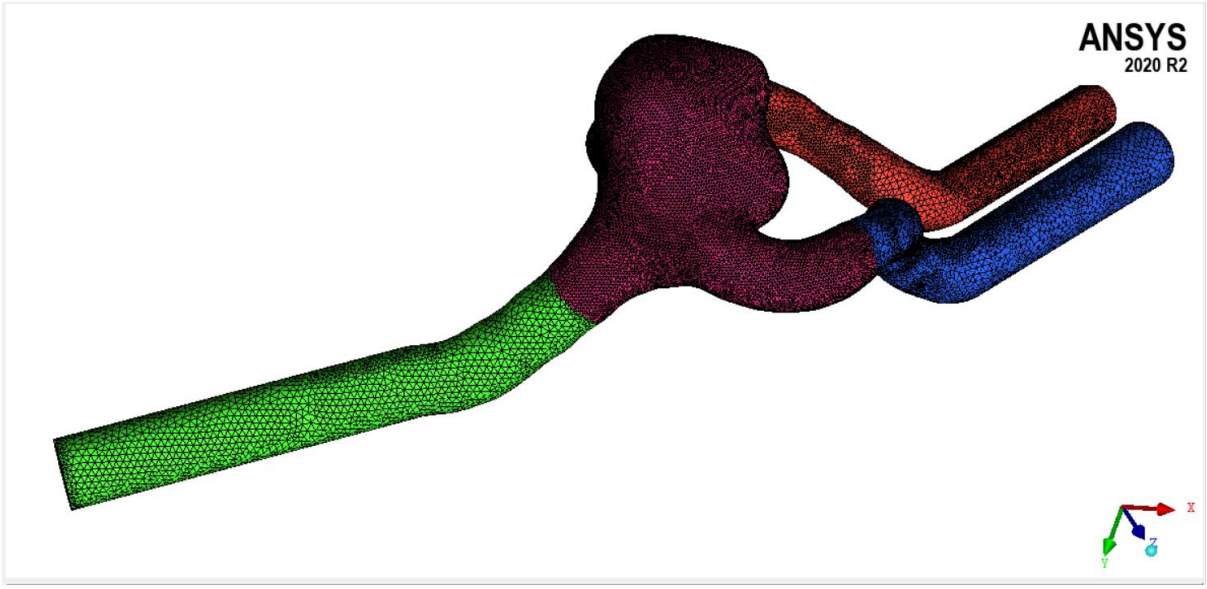

Fig. 3.8: 3D Unstructured Mesh (Total Elements: 15 lacs, Min Quality: 0.45)

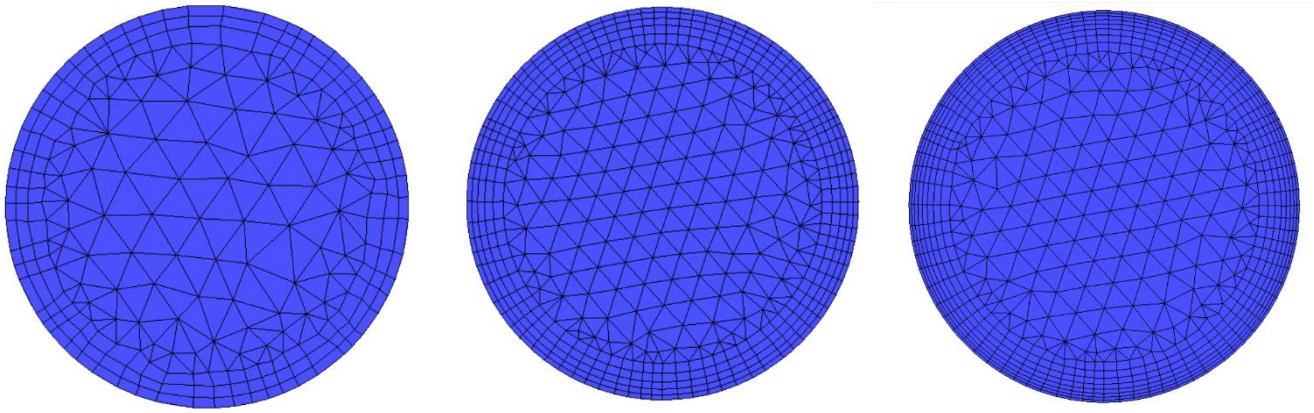

(a) **(b)** **(c)**

Fig. 3.9: (a), (b), and (c) show 3, 5, and 7 Prism Layers at Inlet of ACOM Model

Description: Fig. 3.6, Fig. 3.7, and Fig. 3.8 shows systematic workflow from 3D model extraction to unstructured grid generation.

Mesh Independence: Mesh should be suitable for computational simulation. An unsuitable mesh has badly shaped cells (or elements) that increase the local effective spatial discretization error. However, probably the most common failing of computational meshes for 3D problems is insufficient spatial resolution, leading to inaccurate computation of local velocity and wall shear stress features. For this reason, demonstration of mesh-independence is advocated in the computational fluid dynamics CFD.

Mesh independence refers to a mesh being optimized to have the minimum number of cells to obtain a solution that will not change if any further mesh refinement is made, i.e., the solution becomes independent of the resolution for decreasing element sizes and increasing numbers of cells. This typically involves monitoring a fluid flow parameter of interest, e.g., the velocity or the pressure, under successive grid refinement. In our case, three different grid resolutions are evaluated, where each subsequent mesh is refined. Upon refinement, the grid cells become smaller and the number of cells in the flow domain increases.

Mesh Strategy- A total of three different meshes were tested for the geometry. These meshes included three different global mesh sizes and three different wall prism setups. In **Table 3.3**, Mesh 2 with 5-Prism layers is in bold as it will be used as a reference for the rest of the data comparisons. So, for creating 3 different global size meshes, the scale factor is varied by 1.5 times for coarse to fine mesh i.e. for coarse, medium, and fine mesh global scale factor is 1, 0.66, and 0.44 respectively and the Initial height of prism layer is varied by 2 times so that in 20% of radius we can incorporate 3, 5 and 7 prism layers (see **Fig. 3.9**). In this way, 3 different types of mesh are created (see **Table 3.4**). [(6 lacs, 3P), (15 lacs, 5P) and (44 lacs, 7P)]

Case: Inlet Radius (R_i) = 1.26 mm

Mesh Type	**Global Scale**	**Initial Height (H_i)**	**No. of Prism Layers**
Coarse (M1)	1	H_i	3
Medium (M2)	**0.66**	**H_i/2**	**5**
Fine (M3)	0.44	H_i/4	7

Table 3.3: Grid Independence Strategy

	Size	Initial Height	Height/Growth Ratio	No. of Prism Layers	Total Height
M1	6 lacs	0.063	1.2	3	0.2R
M2	**15 lacs**	**0.0315**	**1.2**	**5**	**0.2R**
M3	44 lacs	0.01575	1.2	7	0.2R

Table 3.4: Grid Parameters for 3 different grids (6L, 15L, and 44L)

	Cell Data
Type	ACOM
Radius	1.26
No. of Nodes	459031
No. of Tetrahedral	8,64,934
No. of Prisms	5,69,075
Total Elements (Cell)	14,34,009

Table 3.5: Mesh Cell Data

	Subject
Total No. of Elements	14,34,009
Non-Orthogonality	12.872
Max Skewness	0.491
Aspect Ratio	3.993

Table 3.6: Mesh Quality Indicators

Table 3.5 and **Table 3.6** represent Mesh Cell data and its quality indicator values for the M2 (15 lacs) mesh.

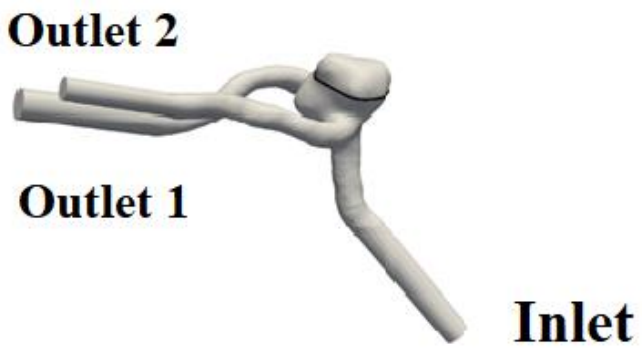

(a)

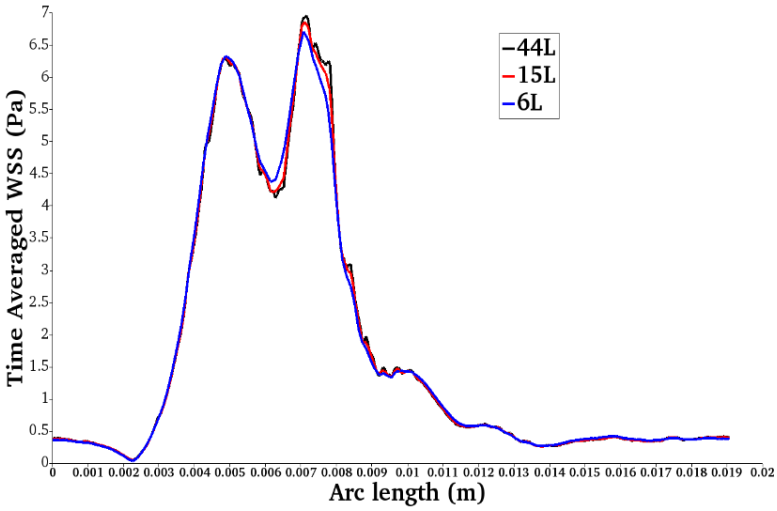

(b) TAWSS

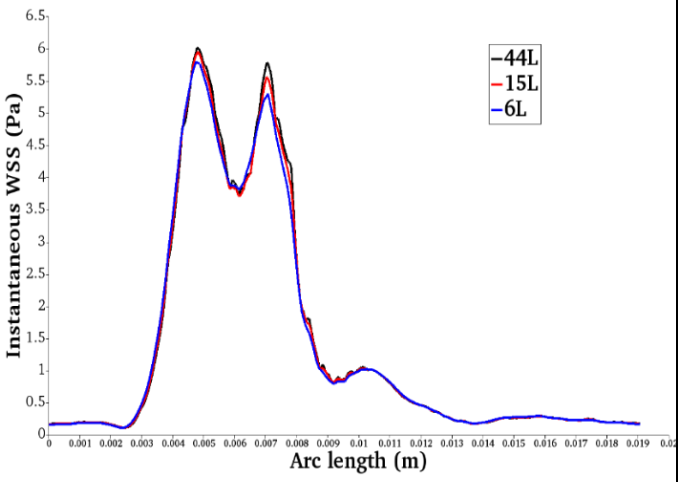

(c) At 1.64 sec (Systole Accelerating)

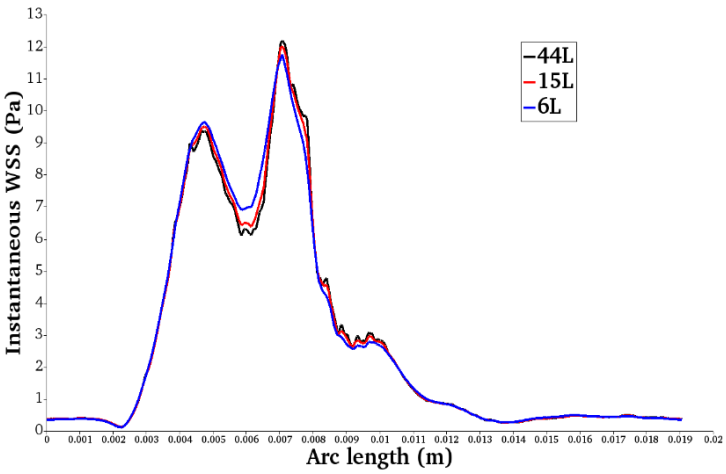

(d) At 1.74 sec time step (Systole)

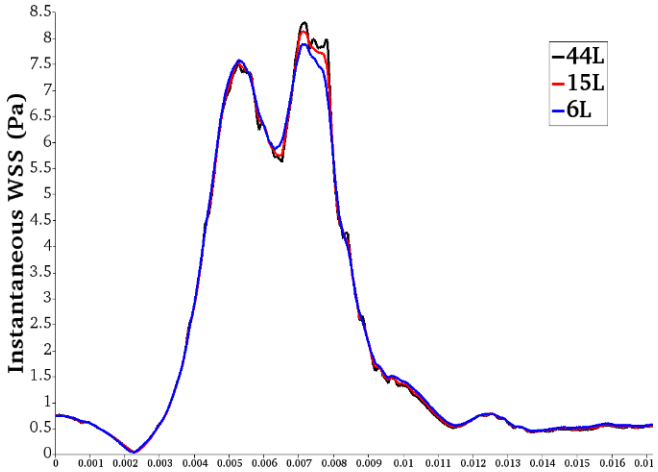

(e) At 2 sec (Systole Deceleration)

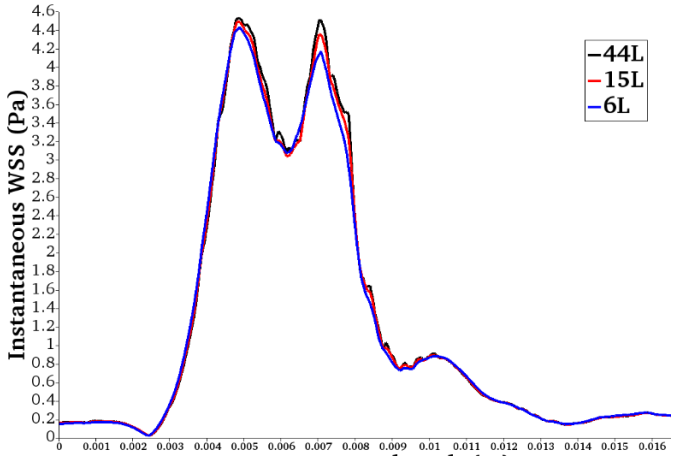

(f) At 2.24 sec (Diastole)

Fig. 3.10: Temporal variation of instantaneous wall shear stress: Mesh Independence study

Fig. 3.10 (a) shows Patient specific geometry of 47 y/o Female with no clinical history of hypertension and heart disease. It is extracted using a 3D slicer and 3 different size volume meshes are created for analyzing CFD results. Time Averaged WSS and Instantaneous WSS results for all 3 meshes at the four different time levels is shown in **Fig. 3.10(c)-(e)**. On X- the axis, Arc length represents that these hemodynamic values are calculated over an arc on the dome of aneurysm geometry. Based on grid independence results we can conclude that M2 (15 lacs) is in good agreement with M3 (44 lacs) during the whole cardiac cycle. Hence, we will use the M2 mesh size for the CFD study.

Conclusion: The optimum mesh size required for accurately resolving the flow dynamics is as defined by the M2(15 lacs element) mesh. This mesh size was found to be in fine agreement with extremely resolved M3 mesh (44 lacs elements) for each cardiac cycle, and thus any further refinement in M2 mesh is computationally expensive for accurate CFD predictions.

3.4 CFD Details

Generally, Governing equations can be discretized by using various techniques namely the finite difference method, the finite volume method, the finite element method, etc. Computational methods help solve complex situations by using available computational resources. Obtaining quick results with better accuracy is very important for the analysis. Most fluid flow software adopts the finite volume technique. Commercial solvers like FLUENT and Open-Source code Open FOAM adopted the finite volume technique. However, Open Foam is an open-source tool providing source code and user friendly. It is a C++ library containing Solvers and Utilities. It has access to pre-processing and post-processing tools. Hence in the present work, Open Foam v-1912 solver is used. Before running the simulations, the solver is validated properly. Numerical simulation was carried out as described previously. The governing equations underlying the calculation were the Navier-Stokes formulations with the assumption of a laminar, homogeneous, and incompressible blood flow. The blood vessel wall was assumed to be rigid with no-slip boundary conditions. The average Reynolds number was within the range of normal blood flow in human cerebral arteries, indicating a laminar flow condition. The density and dynamic viscosity of blood were specified as 1,060 kg/m 3 and 0.0035 N-s/m ^{2}, respectively. The blood flow was assumed to be Newtonian. The overall blood

flow pattern and WSS distribution are relatively independent of the setting of either a Newtonian or a non-Newtonian viscosity.

Boundary Conditions: A no-slip boundary condition is applied at the arterial wall. The blood is allowed to enter with a parabolic velocity profile at the inlet of the computational domain and leaves with zero pressure at the outlet.

$$U = 2 \times U_t \left[1 - \left(\frac{2R}{D}\right)^2\right] \; and \; \frac{\partial P}{\partial n} = 0 \qquad (3.5)\ (At\ Inlet)$$

$$U = 0 \; and \; \frac{\partial P}{\partial n} = 0 \qquad (3.6)\ (At\ Wall)$$

$$\frac{\partial U}{\partial n} = 0 \; and \; P = 0 \qquad (3.7)\ (At\ Outlet)$$

U_t , U, and D are time varying inlet velocity, velocity of blood in z-direction and diameter of normal artery respectively.

Solving Scheme: Using Open FOAM v-1912.The incompressible, transient solver uses the PISO (Pressure-Implicit with Splitting of Operators) algorithm to solve the pressure–velocity decoupling. The second-order accurate upwind scheme is used to discretize the convective terms, while the central differencing scheme is used to discretize the viscous terms. The second-order implicit Euler scheme is used for the discretization of the temporal term. The generalized Geometric-Algebraic Multi-Grid (GAMG) solver with the Gauss-Seidel smoother is used to solve the system of linear equations with an absolute tolerance of 10^{-6} for pressure and 10^{-6} for velocity.

3.5. Post Processing

As a next step, for post-processing purposes ‘ParaView’ software is used. It is free open-source software primarily used for visualization of CFD results in the present study hemodynamic parameters, such as streamlines, WSS, RRT, OSI, etc., are calculated using this software.

CHAPTER 4

RESULTS AND DISCUSSION

Symmetric Vs Asymmetric inlet ACOM Aneurysm: If the A1 segment diameters were similar, with the difference between the 2 less than half of the larger A1 diameter, they were classified as "Symmetric inlet" ACOM aneurysms. Similarly, if the A1 segments showed asymmetry, with the difference between the 2 is greater than half, the smaller vessel was classified as hypoplastic and the larger, as "Asymmetric inlet" ACOM (see **Fig. 4.1**). A1 dominance is an important correlation to the incidence of ACOM aneurysms. This is in agreement with several precedent studies[14]. So present research work includes a comparative study between symmetric inlet ACOM and asymmetric A1 ACOM complex aneurysms for two cases and for each type, two patient-specific geometries were analysed. For all 4 ACOM aneurysms rupture status is pre-defined. This study investigates the reasons behind the rupture of ACOM aneurysm based on well-established post-processed hemodynamic parameters. post-processed hemodynamic parameters.

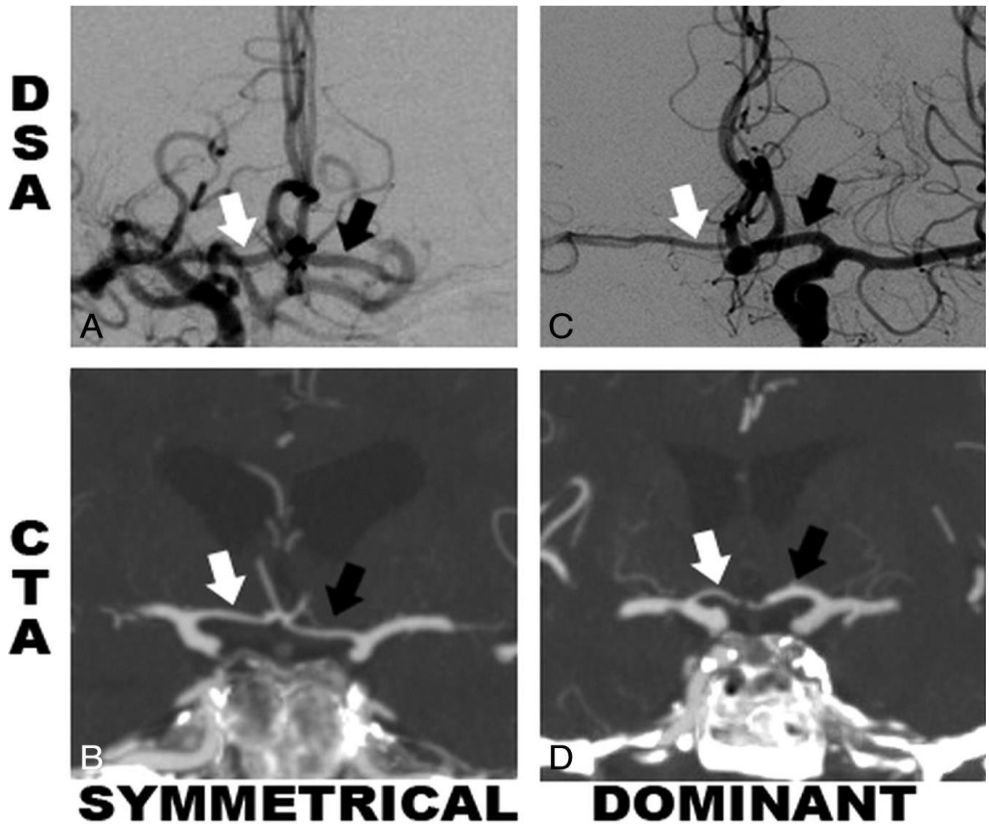

Fig. 4.1: Examples showing A1 segment categories with white and black arrows indicating right and left A1 segments, respectively, for the symmetric and dominant. The "symmetric inlet" configuration from both Die Subtraction Angiography (DSA) and CT Angiography [14]

Streamlines are superimposed with velocity vector and for each ACOM aneurysm at different time-steps of the cardiac cycle streamlines are shown in **Fig. 4.1.** Clinical decision-making 3D images are included for all 4 patients.

Fig. 4.2 (SUB 01 &2) will provide a fair idea of the position and orientation of each computational blood vessel model, characteristic shapes of cerebral aneurysms, and locations of the parent arteries as much as possible. The streamlines are colored according to the magnitude of the blood flow velocity. The patterns of streamlines did not largely change during a cardiac cycle.

Case 01: SUB 01 (Unruptured) and SUB 02 (Ruptured)

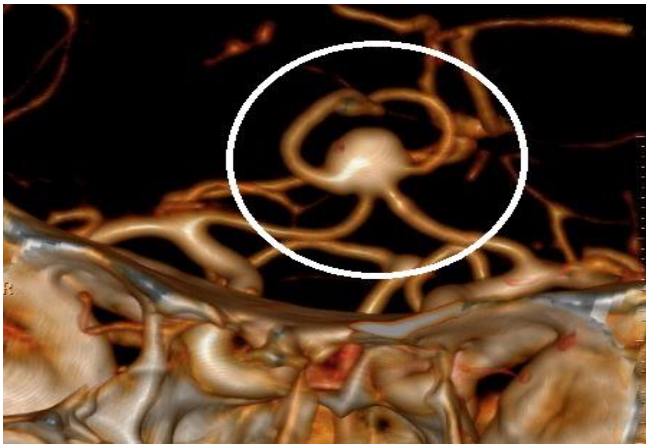

SUB 01

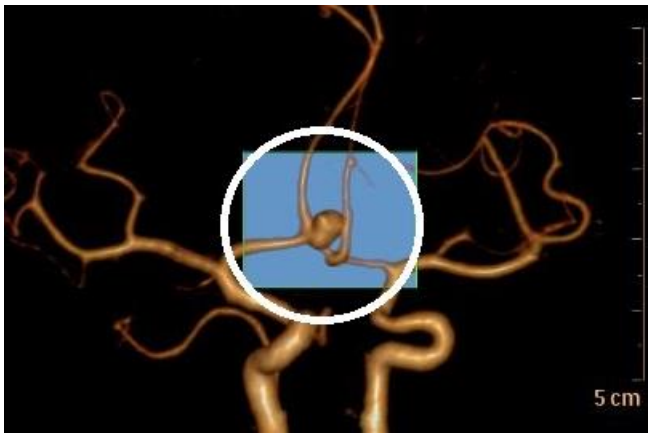

SUB 02

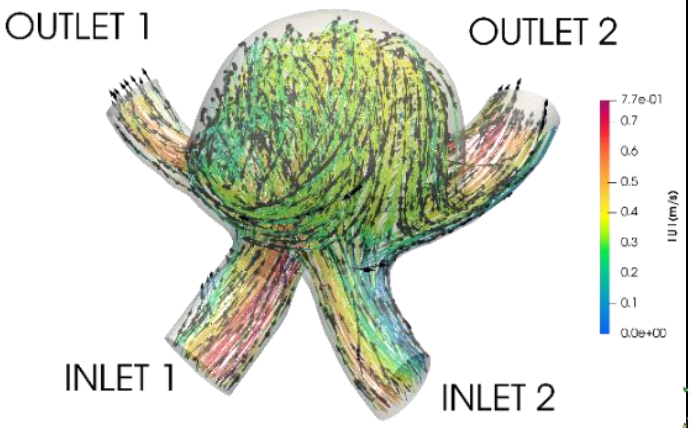

(a) At 1.74 sec

(a*) At 1.74 sec

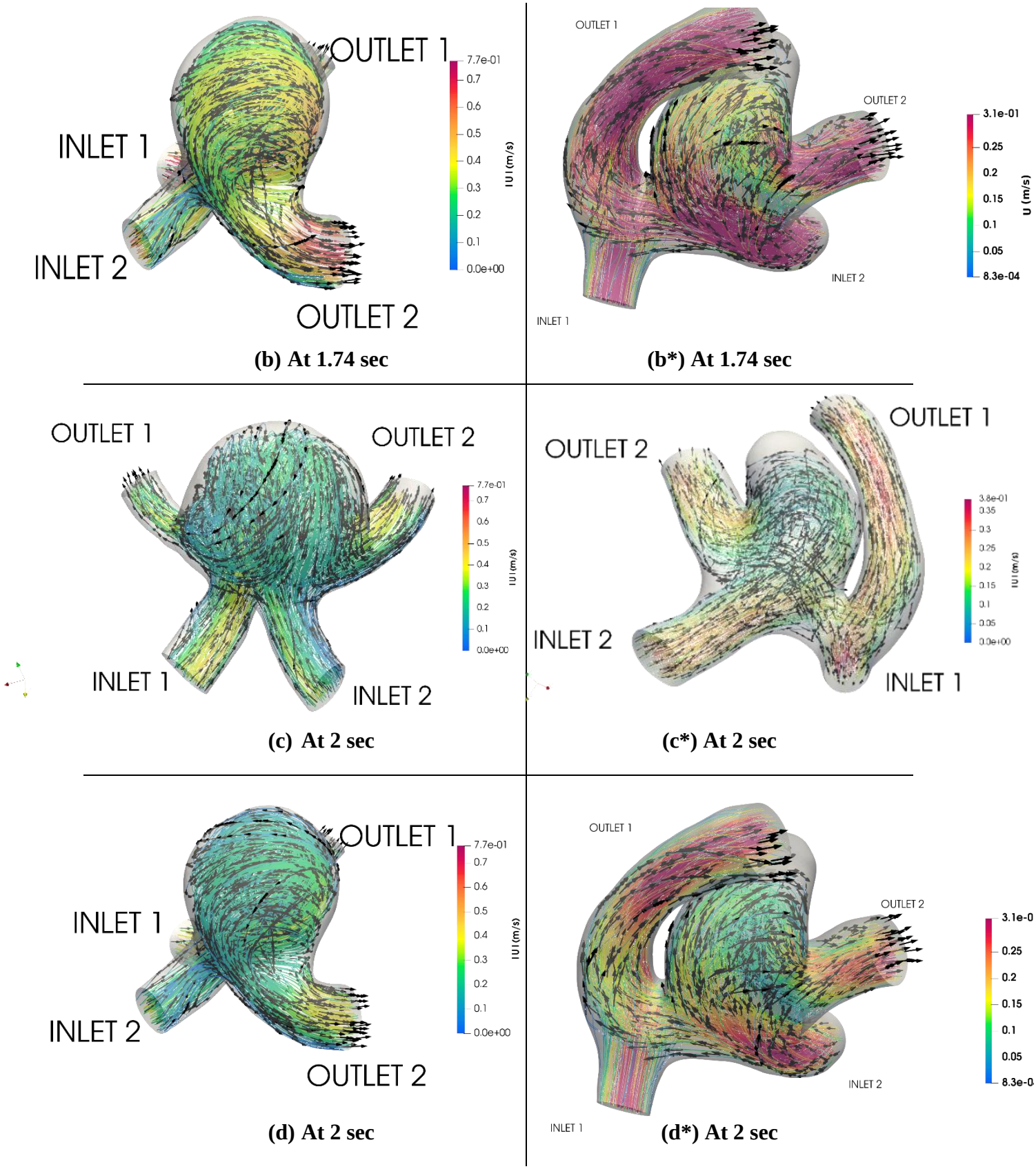

Fig. 4.2: Streamlines (Case 01)

Fig. 4.2 shows flow visualization for symmetric inlet (SUB 01) and A1 asymmetric ACOM(SUB 02) aneurysm at peak systole (1.74 sec) and diastole (2 sec). Frontal and Saggital views are taken for each case. Symmetric inlet ACOM aneurysm(Left) has continuous sliding flow while for A1 asymmetric ACOM complex case(Right), Inlet 2 is dominant, and flow streamlines are directly impinging on the aneurysm dome. The velocity magnitude in the ACOM is less in SUB 02.

Wall Shear Stress: Several parameters were further derived to describe the characteristics of WSS. In the context of pulsatile flow, the WSS magnitude of each element within one cardiac cycle is calculated using the time-averaged WSS [15].

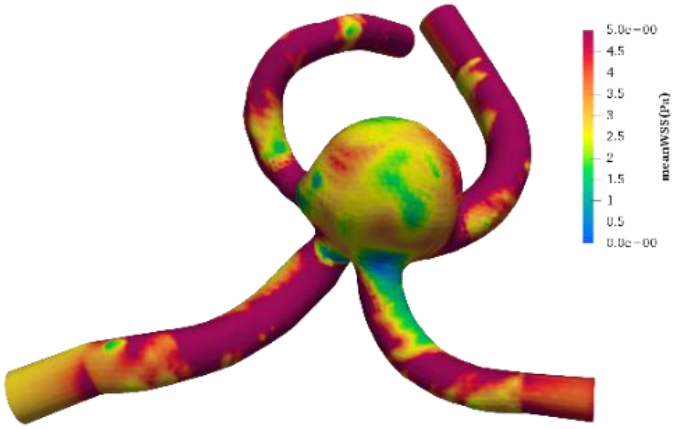

(a) MWSS (2.99 Pa)

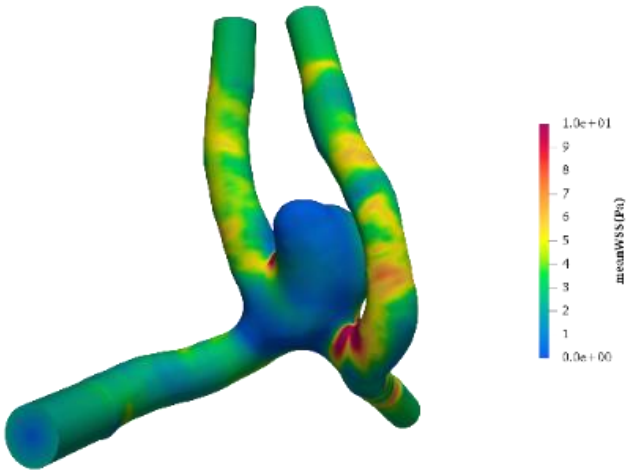

(a*) MWSS (1.1 Pa)

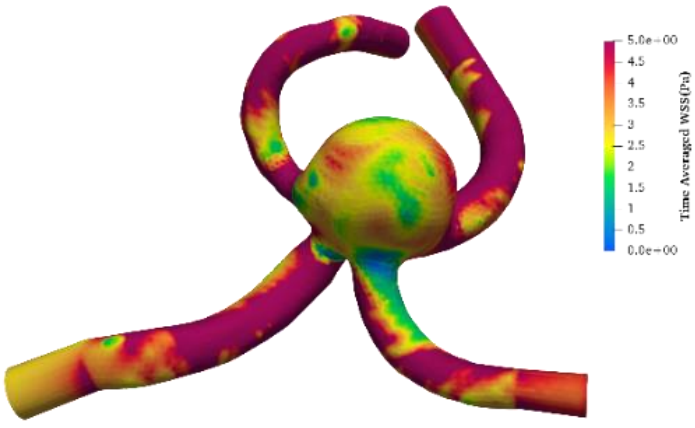

(b) Time Averaged WSS (3.01 Pa)

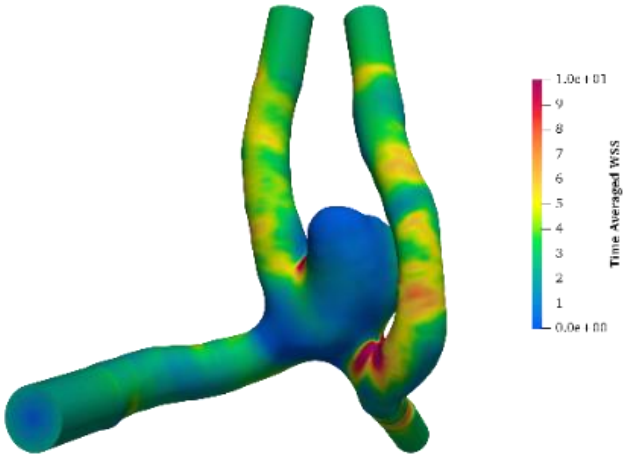

(b*) Time Averaged WSS (1.12 Pa)

Fig. 4.3: WSS Comparison (Case 01)

Fig. 4.3 shows Mean and Time Averaged WSS comparison for symmetric inlet ACOM and A1 asymmetric ACOM case respectively. It is clearly shown that symmetric inlet ACOM (Left) has higher Mean WSS (MWSS) and Time Averaged WSS (TAWSS) in comparison with Asymmetric (Right).

Relative Residence Time: RRT defined as the distribution of blood flow near the proximity of the intra-aneurysmal flow vortex. RRT is an important hemodynamic parameter used to calculate the residence time of blood flow circulating near the aneurysm wall. RRT is used to quantify and differentiate between the thin and thick aneurysm wall regions.[15]

$$RRT = \frac{1}{(1 - 2 \times OSI) \times WSS} \tag{4.1}$$

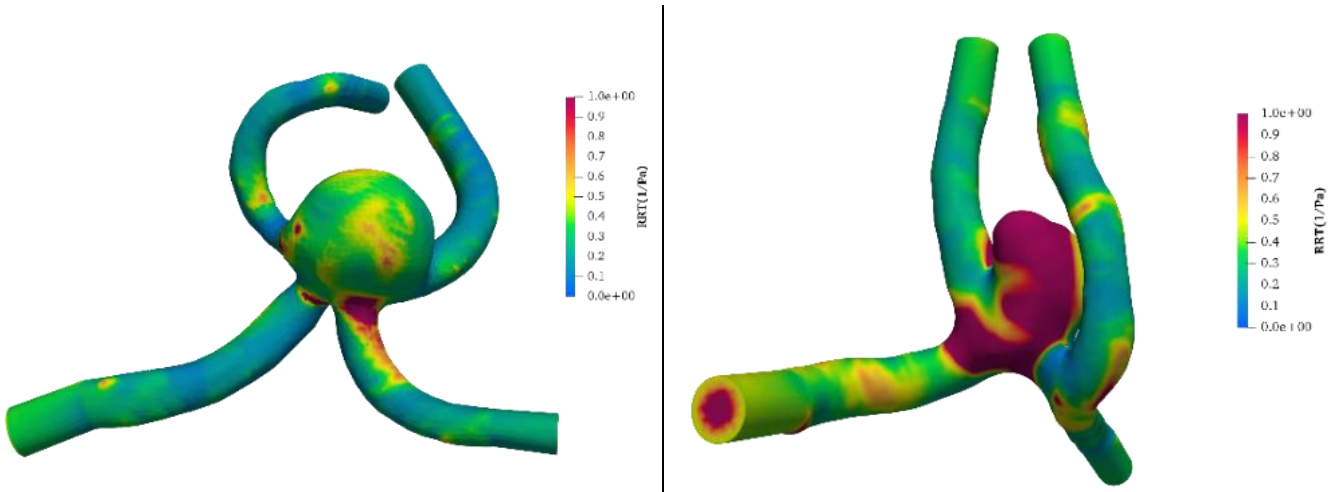

(a) RRT (0.37 Pa^{-1}) **(a*) RRT (2.95 Pa^{-1})**

Fig. 4.4: RRT Comparison (Case 01)

Fig. 4.4 shows RRT distribution over symmetric inlet ACOM and A1 asymmetric inlet ACOM aneurysm, As per the results A1 Asymmetric has higher RRT.

Oscillatory Shear Index: OSI is defined as a strongly oscillating path during a pulsatile flow It is characterized by a nondimensional parameter, and it ranges from 0 to 0.5. wherein 0 represents a steady flow and 0.5 indicates intense oscillatory flow. OSI is often used to describe the disturbance of the flow field in the aneurysm wall. OSI shows the magnitude of WSS changes and it illustrates the tangential oscillation of force as one cardiac cycle function. The equation for OSI is as follows:

$$OSI = \frac{1}{2}\left\{1 - \frac{|\int_0^T WSS_i|\, dt}{|\int_0^T WSS_i\, dt|}\right\} \quad (4.2)$$

where WSS_i is the shear stress vector, and T is the duration of one cardiac cycle.

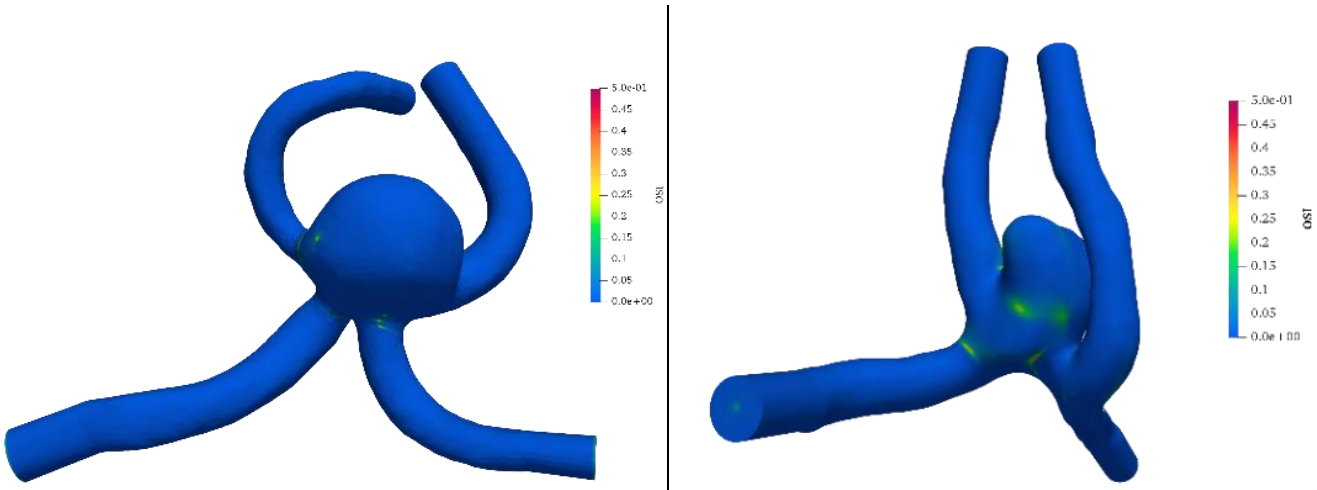

(a) OSI (0.01) **(a*) OSI (0.03)**

Fig. 4.5: OSI Comparison (Case 01)

Fig. 4.5 OSI distribution for A1 asymmetric inlet ACOM is more in comparison to symmetric inlet ACOM aneurysm.

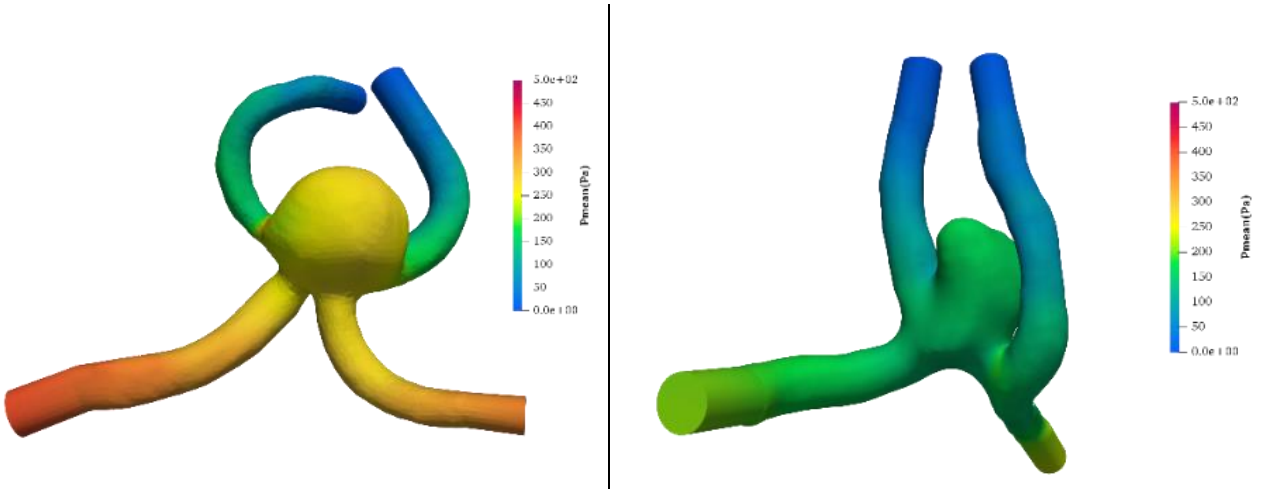

(a) P_{mean} (0.25) **(a*) P_{mean} (0.151)**

Fig. 4.6: P_{mean} Comparison (Case 01)

Fig. 4.6 shows the Spatio-temporal average of pressure on an aneurysm dome. It is more in symmetric inlet ACOM (unruptured) in comparison with A1 asymmetric ACOM(ruptured).

Case 02: SUB 03 (Unruptured) vs SUB 04 (Ruptured)

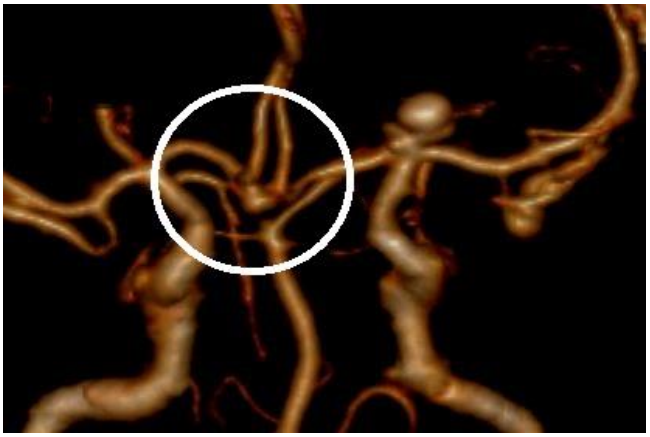

SUB 03

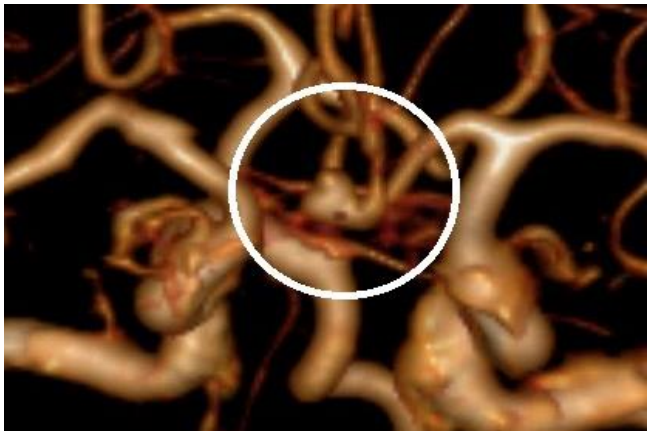

SUB 04

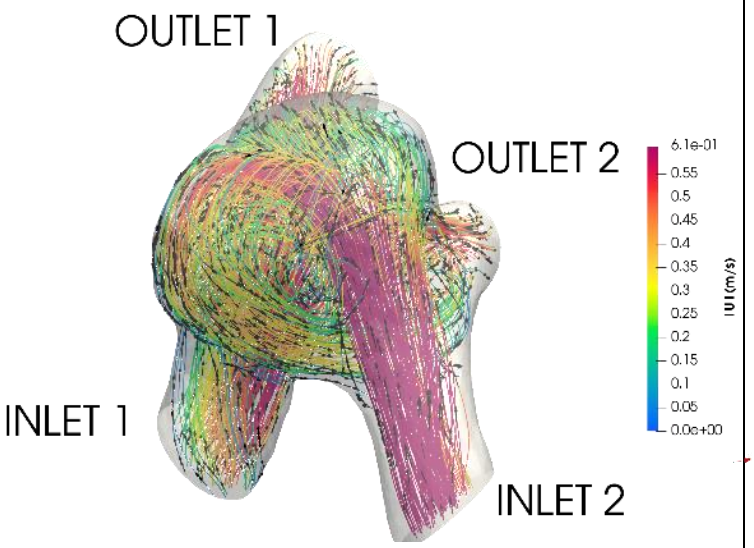

(a) At 1.74 sec

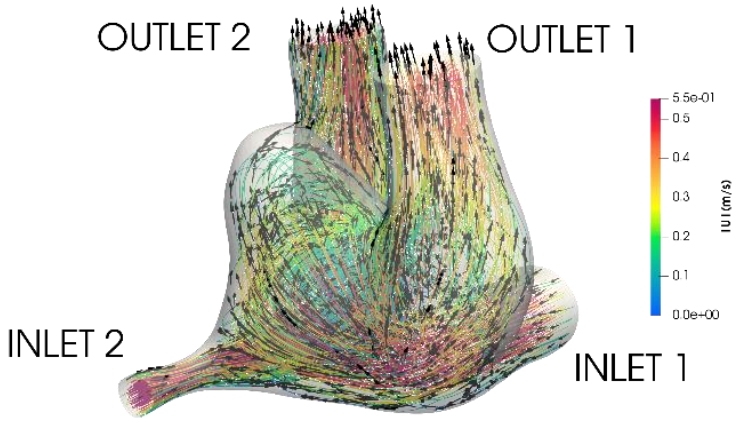

(a*) At 1.74 sec

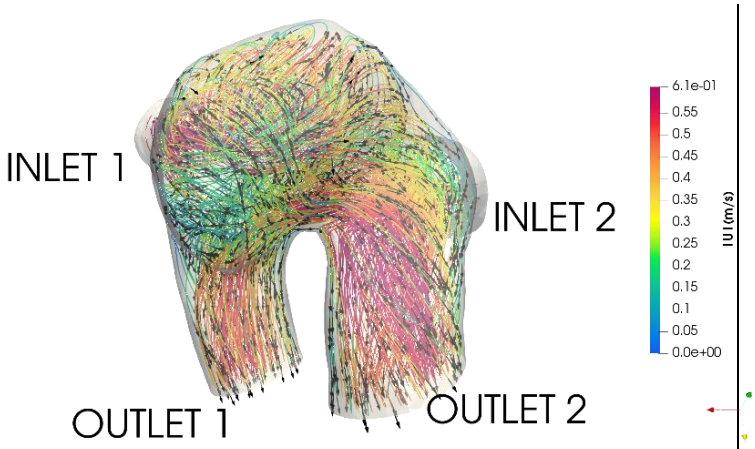

(b) At 1.74 sec

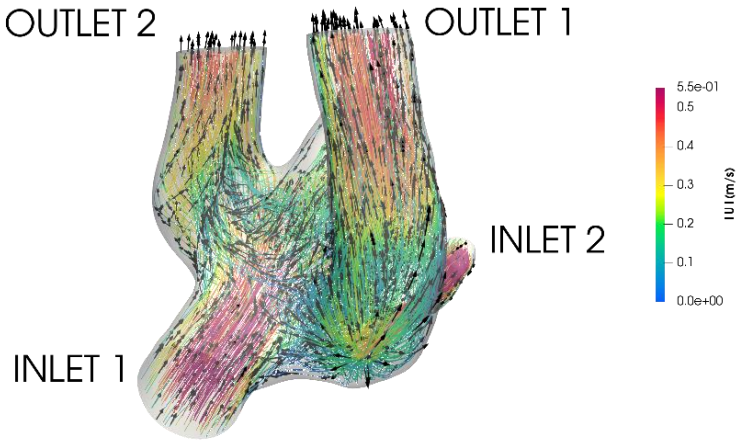

(b*) At 1.74 sec

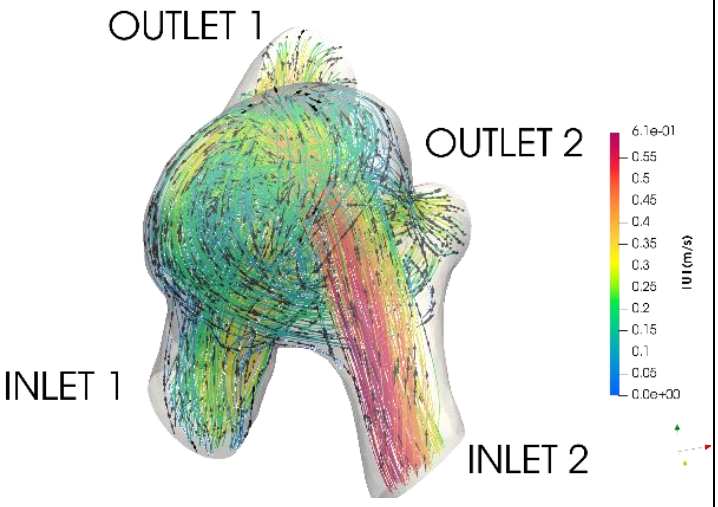

(a) At 2 sec

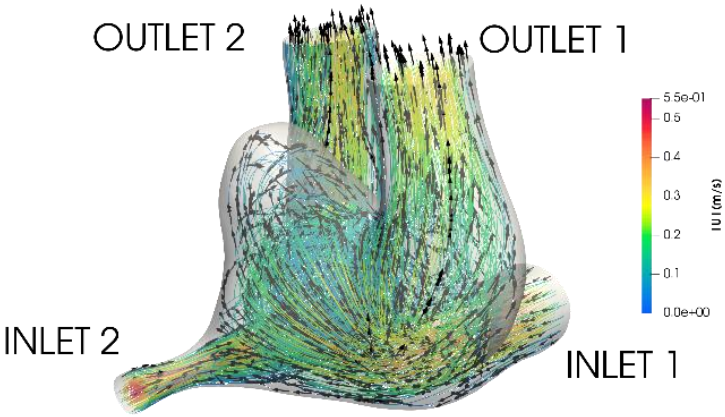

(c*) At 2 Sec

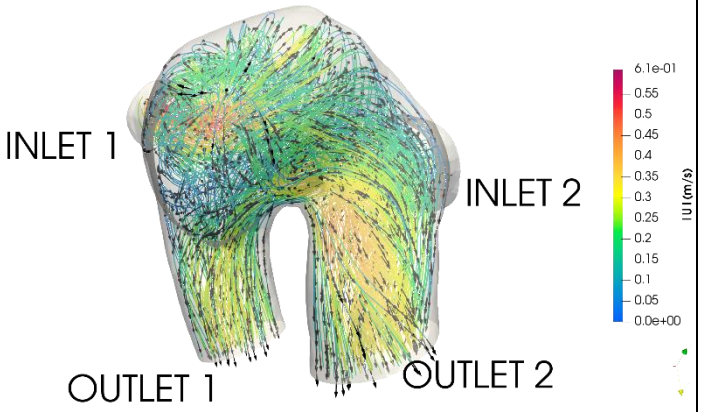

(d) At 2 sec

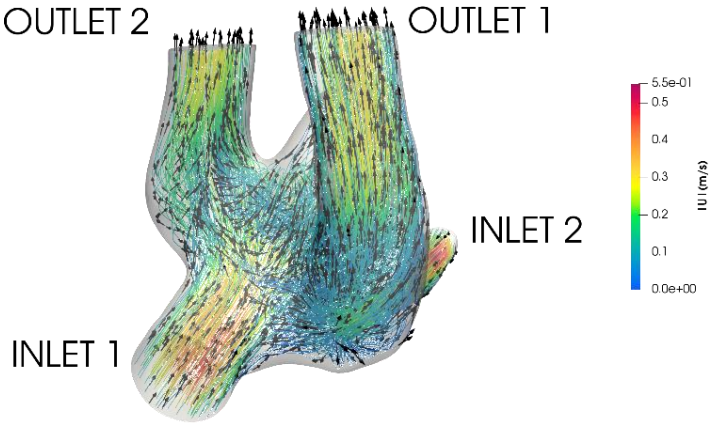

(d*) At 2 sec

Fig. 4.7: Streamlines (Case 02)

Fig. 4.7 shows visualization of streamlimes superimposed with velocity vector for symmetric inlet ACOM (SUB 03) and A1 asymmetric ACOM(SUB 04) aneurysm at peak systole (1.74 sec) and diastole (2 sec). Frontal and Saggital views are taken for each case. Symmetric inlet ACOM aneurysm(Left) has continuous sliding flow while in A1 asymmetric inlet case(Right), Inlet 1 is dominant, and flow streamlines are directly impinging on the aneurysm dome. Also, it is observed that velocity magnitude is higher in symmetric inlet ACOM in comparison with A1 asymmetric ACOM.

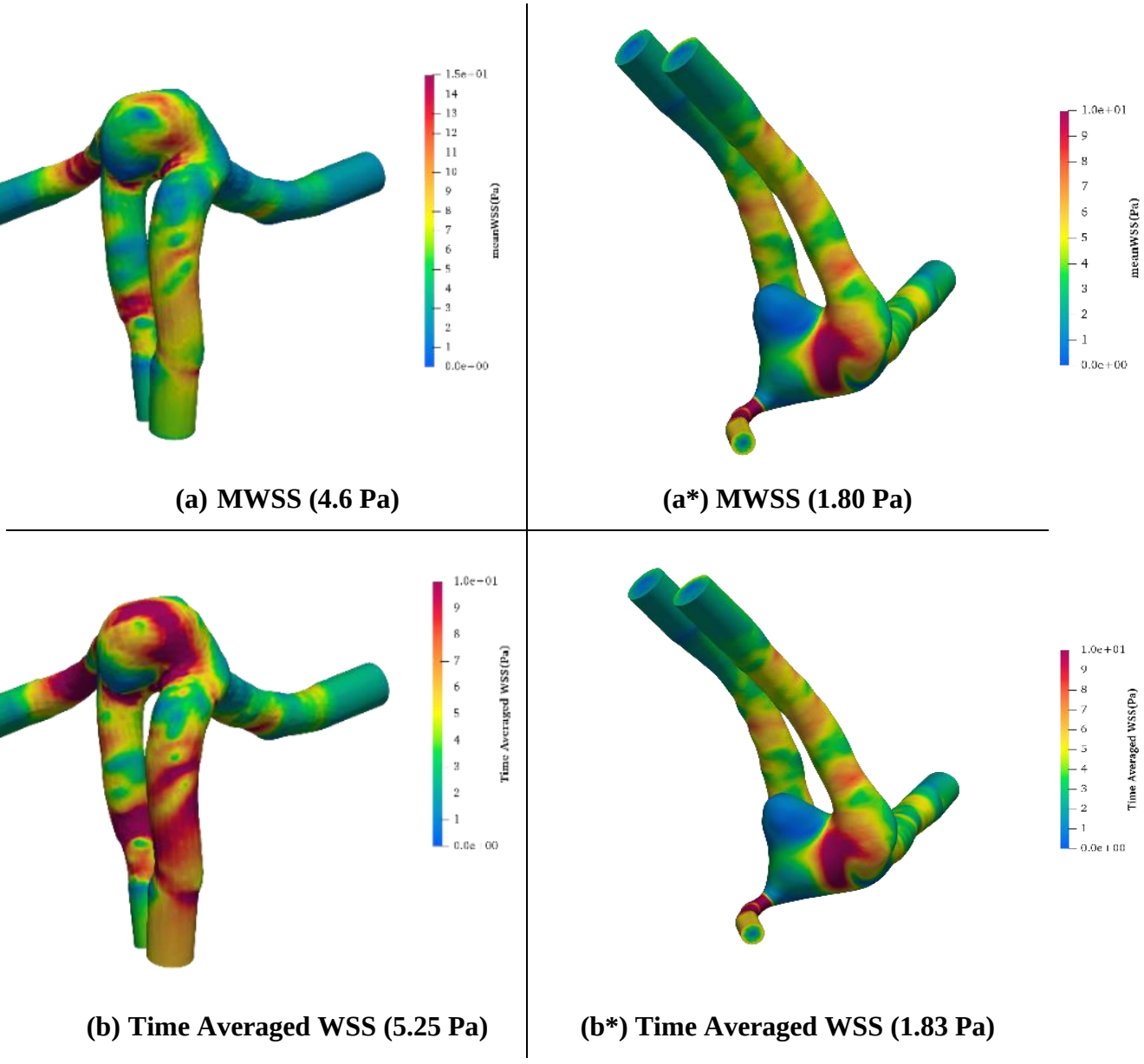

(a) MWSS (4.6 Pa) **(a*) MWSS (1.80 Pa)**

(b) Time Averaged WSS (5.25 Pa) **(b*) Time Averaged WSS (1.83 Pa)**

Fig. 4.8: WSS Comparison (Case 02)

Fig. 4.8 shows Mean and Time Averaged WSS comparison for symmetric inlet ACOM and A1 asymmetric ACOM case respectively. We can clearly distinguish that symmetric inlet

ACOM (Left) has higher Mean WSS and Time Averaged WSS in comparison with A1 asymmetric(Right).

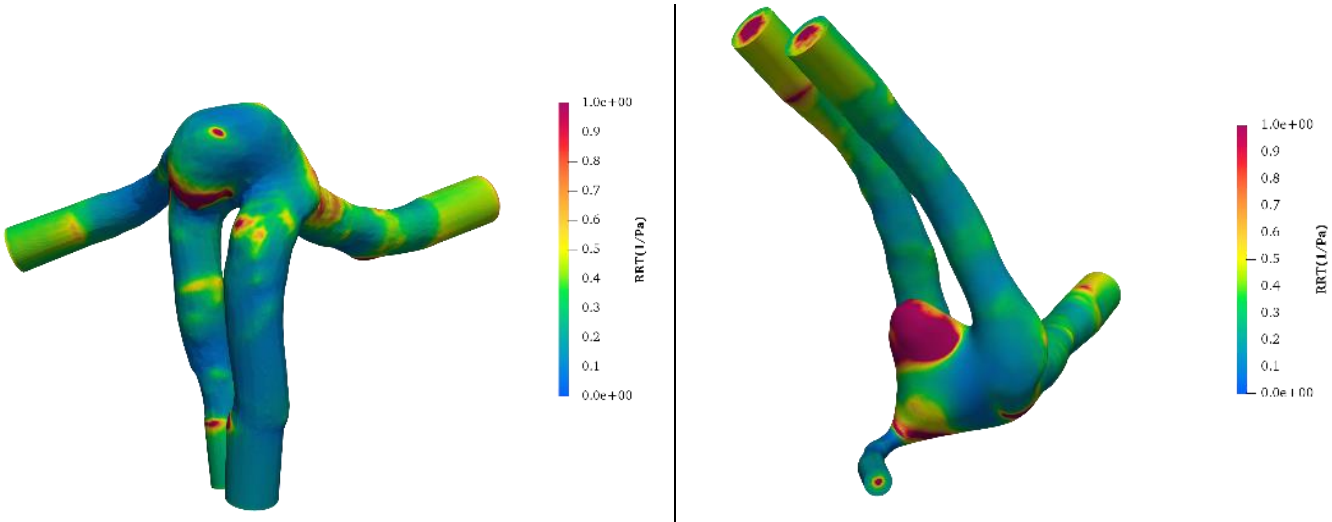

(a) RRT (0.378 Pa^{-1}) **(a*) RRT (0.978 Pa^{-1})**

Fig. 4.9: RRT Comparison (Case 02)

Fig. 4.9 shows RRT distribution over symmetric inlet and asymmetric inlet aneurysm, As per the results A1 asymmetric ACOM case has higher RRT.

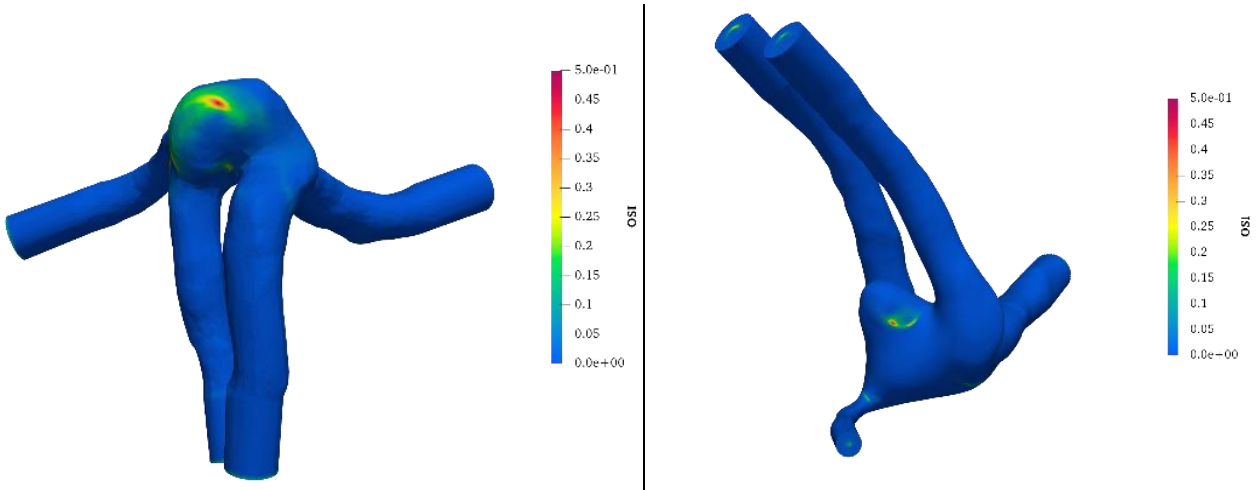

(a) OSI (0.623) **(a*) OSI (0.008)**

Fig. 4.10: OSI Comparison (Case 02)

Fig. 4.10 OSI distribution for asymmetric ACOM is less in comparison to symmetric inlet aneurysm

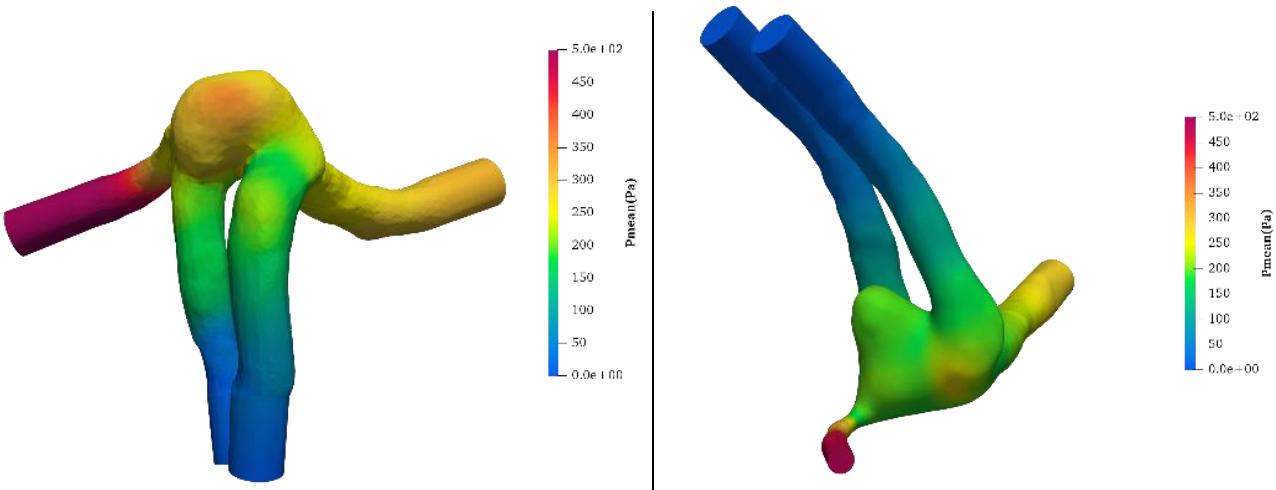

(a) P_{mean} (0.258 Pa) **(a*) P_{mean} (0.184 Pa)**

Fig. 4.11: P_{mean} Comparison (Case 02)

Findings: WSS, the frictional force between blood and aneurysm wall, could use as a parameter to assess the rupture risk. The other important parameter is LSAR. The friction between blood and endothelial cells is essential for normal arterial wall homeostasis. Low or stagnant flow can result in an inflammatory response in the vascular wall. Low WSS was associated with IAs rupture in posterior circulation aneurysms and ACOM aneurysms [12].

- In the present study both symmetric inlet ACOM cases have sliding continuous flow, High Mean Wall Shear Stress and Time Averaged WSS, Less LSAR, and High RRT (see **Table 4.1**) in comparison with A1 asymmetric inlet (Dominant) ACOM cases.
- In A1 asymmetric ACOM cases impingement is on the dome, Low Mean and Time Averaged Wall Shear Stress, High LSAR, and Low RRT values are captured.
- For both symmetric inlet ACOM and A1 asymmetric inlet ACOM aneurysm flow visualization using streamlines are shown (see **Fig. 4.2**,**Fig. 4.7**). It is clear that velocity magnitude and P_{mean} is less for ruptured (**Table 4.1**).
- It may be possible that higher aspect ratios (i.e., narrowed neck ACOM aneurysm) tend to have low WSS and higher RRT values in the dome (**Table 4.1**).
- Our data reflect that aneurysm with low WSS and high LSAR have a high risk of incurring an aneurysm rupture and A1 Asymmetry is an important risk factor for the development of ACOM aneurysm.

	SUB 01 (symmetric inlet ACOM)	SUB 02 (A1 asymmetric inlet ACOM)	SUB 03 (symmetric inlet ACOM)	SUB 04(A1 asymmetric inlet ACOM)
Mean WSS (Pa)	2.99	1.1	4.603	1.801
TAWSS (Pa)	3.01	1.12	5.246	1.83
OSI	0.01	0.03	0.062	0.008
RRT(Pa^{-1})	0.37	2.95	0.388	0.978
GON	0.039	0.11	0.236	0.051
P_{mean} (Pa)	0.25	0.151	0.258	0.184
Max WSS (Pa)	28.5	21.21	19.438	4.26
LSAR (%)	36.37	86.9	19.768	27.69
Aspect Ratio	0.6	0.76	0.55	0.66

Table 4.1:Comparison of Hemodynamic Parameters in symmetric inlet ACOM and A1 asymmetric ACOM Cases

CHAPTER 5
CONCLUSION AND FUTURE WORK

In the present study, computational fluid dynamics-based simulation of the rupture risk of Anterior Communicating Artery Aneurysms (ACOM) is presented. Starting form the Computed Tomography (CT) angiography based dicom images, geometric domains of clinical interest are isolated. Patient-specific computational fluid dynamics (CFD) calculations are performed to obtain detailed hemodynamic parameters. By systematically generating good quality 3D unstructured meshes physiologically relevant fluid flow features are resolved. Specifically, hemodynamic parameters of symmetric inlet and A1 asymmetric inlet ACOM aneurysms are assessed for rupture risk. Polyhedral meshing has shown to have tremendous advantages over tetrahedral meshing concerning the attained accuracy and efficiency of corresponding numerical computations. However, the following limitations may be noted.

- Sometimes during 3D model extraction, the presence of wall artifacts inside the aneurysm geometry can influence the quality of the mesh and finally, the same reflected in the CFD simulations.
- Pre-rupture data will provide more substantial evidence about the reasons behind rupture, which might not be completely reflected in the post rupture based CFD simulations.
- The present study did not provide patient-specific pressure boundary conditions at the distal end of the outlets.

Scope for future work

- A detailed study on a large number of patient specific geometries would reveal comparison among A1 asymmetric inlet and symmetric inlet ACOM cases, which will strengthen the rupture hypothesis.

REFERENCES

.

[1] Y. Murayama, S. Fujimura, T. Suzuki, and H. Takao, "Computational fluid dynamics as a risk assessment tool for aneurysm rupture," *Neurosurgical Focus*, vol. 47, no. 1, Jul. 2019, doi: 10.3171/2019.4.FOCUS19189.

[2] G. X. Wang *et al.*, "A simple scoring model for prediction of rupture risk of anterior communicating artery aneurysms," *Frontiers in Neurology*, vol. 10, no. MAY, pp. 1–7, 2019, doi: 10.3389/fneur.2019.00520.

[3] L. Sheh Hong, M. Azrul Hisham Mohd Adib, M. Uzair Matalif, M. Shafie Abdullah, N. Hartini Mohd Taib, and R. Hassan, "Modeling and Simulation of Blood Flow Analysis on Simplified Aneurysm Models," *IOP Conference Series: Materials Science and Engineering*, vol. 917, no. 1, 2020, doi: 10.1088/1757-899X/917/1/012067.

[4] K. Tanaka *et al.*, "Relationship between hemodynamic parameters and cerebral aneurysm initiation," *Proceedings of the Annual International Conference of the IEEE Engineering in Medicine and Biology Society, EMBS*, vol. 2018-July, pp. 1347–1350, 2018, doi: 10.1109/EMBC.2018.8512466.

[5] W. Kaspera *et al.*, "Morphological, hemodynamic, and clinical independent risk factors for anterior communicating artery aneurysms," *Stroke*, vol. 45, no. 10, pp. 2906–2911, 2014, doi: 10.1161/STROKEAHA.114.006055.

[6] E. Marchandise, P. Crosetto, C. Geuzaine, J. F. Remacle, and E. Sauvage, "Quality open source mesh generation for cardiovascular flow simulations," *Modeling, Simulation and Applications*, vol. 5, no. Simbio, pp. 395–414, 2012, doi: 10.1007/978-88-470-1935-5_13.

[7] S. Prakash and C. R. Ethier, "Requirements for mesh resolution in 3D computational hemodynamics," *Journal of Biomechanical Engineering*, vol. 123, no. 2, pp. 134–144, 2001, doi: 10.1115/1.1351807.

[8] J. R. Nanduri, F. A. Pino-Romainville, and I. Celik, "CFD mesh generation for biological flows: Geometry reconstruction using diagnostic images," *Computers and Fluids*, vol. 38, no. 5, pp. 1026–1032, 2009, doi: 10.1016/j.compfluid.2008.01.027.

[9] R. Kwak, “Hemodynamics of Willis Aneurysms Angiography in the Anterior Part of the Circle in Patients with : A Study by Intracranial Cerebral Division of Neurosurgery , Institute of Brain Diseases , Tohoku University School of Medicine , Sendai 980 We have already ,” pp. 69–73, 1980.

[10] R. Jabbarli *et al.*, “Clinical relevance of anterior cerebral artery asymmetry in aneurysmal subarachnoid hemorrhage,” *Journal of Neurosurgery*, vol. 127, no. 5, pp. 1070–1076, 2017, doi: 10.3171/2016.9.JNS161706.

[11] M. A. Castro, C. M. Putman, M. J. Sheridan, and J. R. Cebral, “Hemodynamic patterns of anterior communicating artery aneurysms: A possible association with rupture,” *American Journal of Neuroradiology*, vol. 30, no. 2, pp. 297–302, 2009, doi: 10.3174/ajnr.A1323.

[12] P. Jiang *et al.*, “A novel scoring system for rupture risk stratification of intracranial aneurysms: A hemodynamic and morphological study,” *Frontiers in Neuroscience*, vol. 12, no. SEP, pp. 1–12, 2018, doi: 10.3389/fnins.2018.00596.

[13] H. Meng, V. M. Tutino, J. Xiang, and A. Siddiqui, “High WSS or Low WSS? Complex interactions of hemodynamics with intracranial aneurysm initiation, growth, and rupture: Toward a unifying hypothesis,” *American Journal of Neuroradiology*, vol. 35, no. 7, pp. 1254–1262, 2014, doi: 10.3174/ajnr.A3558.

[14] E. Tarulli and A. J. Fox, “Potent risk factor for aneurysm formation: Termination aneurysms of the anterior communicating artery and detection of A1 vessel asymmetry by flow dilution,” *American Journal of Neuroradiology*, vol. 31, no. 7, pp. 1186–1191, 2010, doi: 10.3174/ajnr.A2065.

[15] M. A. A. Sheikh, A. S. Shuib, and M. H. H. Mohyi, “A review of hemodynamic parameters in cerebral aneurysm,” *Interdisciplinary Neurosurgery: Advanced Techniques and Case Management*, vol. 22, no. March, p. 100716, 2020, doi: 10.1016/j.inat.2020.100716.